GENERATING BEAMS OF POLARIZATION ORDER NUMBER +1 USING A CELLOPHANE SHEET

JOHNSTON KAMUTI KALWE

MASTER OF SCIENCE

(Physics)

JOMO KENYATTA UNIVERSITY OF

AGRICULTURE AND TECHNOLOGY

2015

Generating beams of polarization order number +1 using a cellophane sheet

Johnston Kamuti Kalwe

A thesis submitted in partial fulfillment for the degree of Master of Science in Physics of Jomo Kenyatta University of Agriculture and Technology

2015

DECLARATION

This thesis is my original work and has not been presented for degree award in any other university.

Signature ……..…..……. Date …….

JOHNSTON KAMUTI KALWE

This thesis has been submitted for examination with our approval as university supervisors.

1. Signature ……..…..……. Date …….

PROF. GEOFFREY KIHARA RURIMO

JKUAT, KENYA

2. Signature ……..…..……. Date …….

DR. CALVINE FUNDI OMINDE

JKUAT, KENYA

DEDICATION

I dedicate my entire work to my parents Mr. Paul Kalwe Kyondo and Mrs. Mary Mwikali Kalwe for their love, encouragement, unsurpassed efforts and ever commitment to my life. Thank you so much for being so dear to me. I am proud of you and I love you. May God richly bless you, give you peace at heart and increase your boundaries to surpass all human understanding.

ACKNOWLEDGEMENT

First of all I would like to thank the Almighty God in who I have found sufficient grace to go through this course successfully. He has made my dream and vision come true.

I record my special and heartfelt gratitude to my first Supervisor Dr. G. Kihara Rurimo for his guidance in every aspect of this thesis. His quick mind, broad knowledge in optics and lasers and the "can-do" attitude have set a great example for me to follow. His constant encouragement over the years, even for minor achievements, has given me great confidence in pursuing my Masters degree. I doubt that I will be able to convey my appreciation fully, but I owe him my eternal gratitude.

I would like to thank my second Supervisor, Dr. Calvine F. Ominde for his continuous guidance and tireless support. He taught me basically everything in the lab, from optics alignment and at numerous times helped me out of many "traps" that I had fallen into. I consider myself lucky to have had such a wonderful supervisor.

A very special thank to Jomo Kenyatta University of Agriculture and Technology through Dr. Githiri, the Chairman Physics Department, academic and the technical staff for creating a comfortable and open environment for my research. You have constantly given me constructive suggestions for experiments and your administrative advice was a great resource whenever I consulted you. I would also like to acknowledge Lydia Gikonyo, the department of Physics secretary for her support during my research.

I owe special thanks to Prof. Gerd Leuchs and Dr. Peter Banzer for their hospitality during the time I spent in the Leuchs Division, INMik research group at the Max Planck Institute for the Science of light, MPL Germany. The support and conducive environment you provided made my live and stay in Erlangen more bearable and fulfilling.

I am most grateful to Martin Neugebauer whom I closely worked with. He guided this research at every stage with clarity and the rare gift of “getting things done”. I sincerely congratulate him.

To all the colleagues in the INMiK group, thanks for all that I learned through the group presentations and discussions. It was great to spend time together and have moments of fun. I wish you all a successful and a pleasant time in your PhD programmes.

To my siblings; Penninah, Felix, Fredrik and Valentine, thanks for your love, support, concern and prayers that have remained real to me. And to my beautiful niece, Michelle Ndanu, congratulations on the safe arrival. May you find babyhood a wonderful and rewarding experience. Long live!

To my good friend and confidant, Jacqueline Mutheu, thank you for being there for me at all times. I cherish your company and the support you have given me. We have surely made it together.

I highly appreciate the funding of my Masters of Science programme by both the Kenyan Higher Education Loan Board, HELB through the post graduate partial scholarship programme and the German government through the *Deutsche Akademische Austauch Dienst*: DAAD in-country scholarship.

Finally, I am most grateful to the many people whom I worked with on this research for their encouragement and good company. It would have been hard to bear without you.

TABLE OF CONTENTS

LIST OF FIGURES

LIST OF TABLES

LIST OF APPENDICES

ABBREVIATIONS

CAD	Computer Aided Design
CCD	Charged coupled device camera
Cello	Cellophane sheet
CL	Collimating lens
CV	Cylindrical Vector
DF	Density filter
FL	Focusing lens
HWP	Half Waveplate
KSh	Kenya Shillings
LC	Liquid Crystal
LG	Laguerre Gaussian
Lp	Linear polarizer
LPSF	Lens Pinhole Spatial Filter
MO	Microscope objective
NA	Numerical Aperture
OI	Optical diode
PBS	Polarizing Beam Splitter
PC	Polarization converter

PD	Photodiode
PH	Pinhole
PM	Power meter
PMF	Polarization maintaining fibers
QWP	Quarter WavePlate
SVR	Spatially Varying Retarder
TEM	Transverse Electromagnetic

LIST OF SYMBOLS

c-	Crystallographic axis
CO_2	Carbon dioxide
Nd:YAG	Neodymium Yttrium Aluminium Garnett
SiO_2	Silicon (IV) Oxide
Ta_2O_5	Tantalum pent oxide
YVO_4	Yttrium Vanandate Oxide
η	Refractive index
λ	Wavelength
φ	Phase Difference
ω	Angular frequency

ABSTRACT

Beams with polarization order number +1 represent radially or azimuthally polarized light beams. These polarization tailored beams have attracted immense attention in a wide array of scientific and technological disciplines due to their unique properties and potential applications in material processing, optical trapping, and optical data storage among many others. Numerous techniques investigated in the past for obtaining these beams have had certain difficulties. For example, the use of conical elements involved difficult and/or impractical refractive index matching techniques. Other methods reported are very expensive, cumbersome and even difficult to realize in practice. Contrary to these techniques, this research presents a robust, simple, cost effective and practical method of obtaining these beams using a cellophane sheet. The research began with a search for a cellophane sheet with birefringence property. Using a polariscope test, various cellophane sheets were tested. The sheet that displayed the largest variation in the transmitted light with rotation was selected and used for the fabrication of a polarization mask which consisted of four segments. The fast axis of each segment was oriented differently in order to rotate locally the polarization of the incident linearly polarized beam as desired. To ensure the correct operation of the polarization mask, the polarization state of the generated beam was tested by measuring the spatial distribution of the Stokes parameters. A frequency stabilized He-Ne laser operating at a wavelength λ = 632.8 nm was used as the source of light. The light beam was spatially filtered, expanded and then collimated. It was then passed through the fabricated polarization mask, which converted the linearly polarized beam into either a pseudo-radially or a pseudo-azimuthally polarized beam. To achieve a high mode purity of the generated beams, higher order modes were filtered out utilizing a spatial filter. To ensure that the beam emerging from the polarization mask was indeed radially or azimuthally polarized, it was passed through a rotating linear polarizer. The resulting image patterns or lobes were captured using a CCD camera interfaced with a computer. The number and the positions of the lobes agreed with the theoretical predictions. The polarization purity of generated and filtered radially polarized beam was quantified by performing a set of

measurements and thereby calculated the Stokes parameters S_0, S_1, S_2, S_3. In addition, the spatial distributions of the experimentally normalized Stokes parameters S_0, S_1, S_2, S_3 of the filtered radially polarized beam were obtained and compared with the theoretically expected distributions. These (experimentally obtained) distributions were comparable with their respective theoretically calculated distributions; an indication that the beams generated using the cellophane-made converter is of good mode quality.

CHAPTER ONE

1.0 INTRODUCTION AND LITERATURE REVIEW

1.1 Background of the study

Polarization is specific characteristic of transverse waves such as light and other electromagnetic (EM) waves. It involves the vectorial nature of light (Martinez-Herrero *et al.,* 2009). By convention, the polarization of light is described by specifying the orientation of the electric field over one period of oscillation. For the case of a plane wave propagating in free space, the polarization is perpendicular to the direction of propagation and 2-degrees of freedom remain for the orientation of the electric field. Usually, one discriminates between three different types of polarization i.e., linear, circular or elliptical polarization.

The concept of polarization order is useful for understanding the spatial polarization distribution of higher order beam modes. The polarization order number refers to the number of complete polarization rotations per round trip i.e., 0 to 2π. For beams with polarization order number +1 (radially or azimuthally polarized), the field at the focal plane is maximum at the center for the longitudinal polarization and zero for the transversal field whereas for beams with polarization order number -1, both transversal and longitudinal polarizations are zero at the center and non-zero around the center (Pereira & Van-de-Nes, 2004). Different names derived from the characteristics of these beams have been used in literature. Names like cylindrical vector (CV) beams due to their cylindrical symmetry in amplitude and polarization (Youngworth & Brown, 2000; Kozawa & Sato, 2005) and doughnut beams due their characteristic ring shape in intensity (Stalder & Schadt, 1996; Quabis *et al.,* 2000; Pereira & Van-de-Nes, 2004) are common.

These beams have attracted much attention in a wide range of scientific and technological disciplines due to their unique properties and potential applications. For their successful applications, a full characterization of the mode profiles as well as their

polarization state is essential (Kindler *et al.,* 2007; Yuhzao, 2009). For instance, when a beam with radial polarization is focused using a high numerical aperture (NA) system, an intense longitudinal component of the electric field results in the focal region (Scully & Zubairy, 1991). This longitudinal field has been confirmed in various publications (Quabis *et al.,* 2000; Youngsworth & Brown, 2000; Biss & Brown, 2001; Quabis *et al.,* 2001; Dorn *et al.,* 2003; Miyaji *et al.,* 2004; Pereira & Van-De-Nes, 2004; Rurimo *et al.,* 2006). Also, the influence of polarization on the shape of the focal spot has experimentally been verified where a smaller spot size in comparison to a linearly polarized beam has been reported (Quabis *et al.,* 2000; Dorn *et al.,* 2003). Because of these properties, radially polarized beams have found applications in optical data storage (Xiangping *et al.,* 2011) and laser machining (Niziev & Nesterov, 1999; Krishnan & Tan, 2012). Furthermore, both tightly focused azimuthally and radially polarized light beams have proven to be versatile tools in the field of optical trapping (Zhan, 2004; Kozawa & Sato, 2010), microscopy (Hao *et al.,* 2010) and nanoplasmonics (Kindler *et al.,* 2007; Sancho-Parramon & Bosch, 2012).

This interest in radially and azimuthally polarized beams has fostered the development of many different techniques on how to generate these beams. For instance, a polarization state with cylindrical symmetry can be prepared inside a laser cavity, for example by using binary dielectric diffraction gratings or a conical Brewster prism (Kozawa & Sato, 2005; Moser *et al.,* 2006). External methods have also been utilized where specially designed polarization converters such as segmented commercial wave plates have been used to rotate the polarization state locally (Quabis *et al.,* 2005; Machavariani *et al.,* 2007; Maekawa & Uesaka, 2008). Additionally, interferometric arrangements that involve coherent superposition of linearly polarized beams are utilized (Scully & Zubairy, 1991; Tidwell *et al.,* 1990; Stalder & Schadt, 1996; Oron *et al.,* 2000; Neil *et al.,* 2002; Passily *et al.,* 2005; Maurer *et al.,* 2007; Zhan, 2009). Each of these methods has its own drawbacks, especially when considering the cost factor.

For this research, the concept of sectored spatially varying retarder (SVR) is further developed with regards to cost efficiency. For that, the procedure for fabricating a low-cost polarization mask consisting of four segments of Cellophane is described. The Cellophane sheets used were obtained locally and each tested for the birefringence property. Such a device is very cost-efficient and allows for the generation of beams with polarization order number +1. Additionally, Cellophane sheet was chosen as an optical material in this research because of its flexibility especially in designing new optical components that are easily achievable and cost effective.

1.2 Background of polarization and beams with polarization order number +1

Beams with polarization order number +1 including radial and azimuthal have ring type intensity distribution as illustrated in figure 1.1. In the case of radial (azimuthal) polarization, the direction of the electric vector in the plane of the beam cross section is parallel (perpendicular) to the radial direction (Nesterov & Niziev, 2000). Both radially and azimuthally polarized beams can be expressed as a coherent summation of TEM_{10} and TEM_{01} modes as depicted in figure 1.1. A $y-$polarized TEM_{10} mode and $x-$polarized TEM_{01} mode gives an azimuthally polarized beam whereas a $x-$polarized TEM_{10} mode and $y-$polarized TEM_{01} mode produces a radially polarized beam (Tidwell *et al.,* 1990; Nesterov & Niziev, 2000; Niziev *et al.,* 2006).

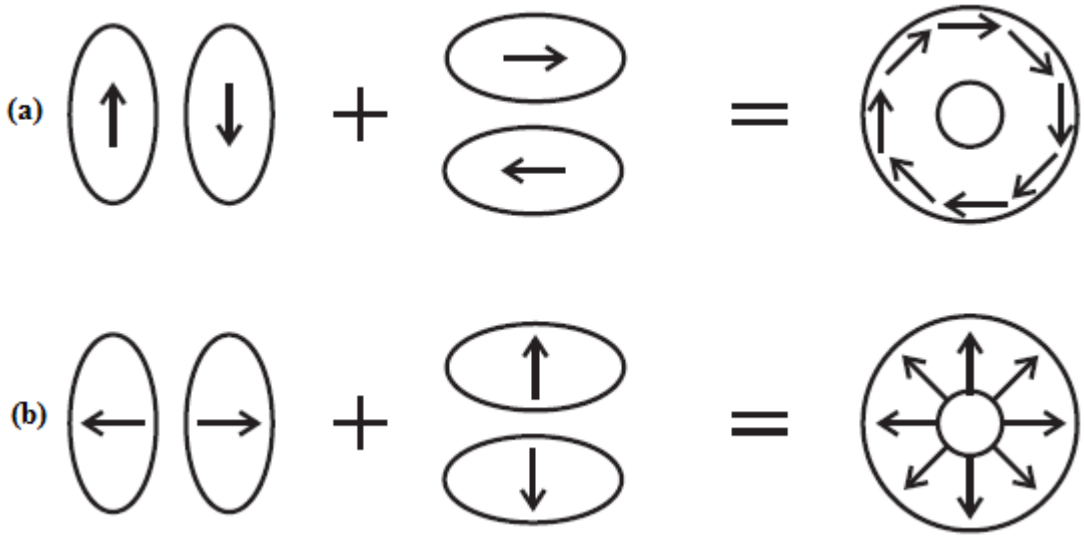

Figure 1.1: Synthesis of different polarization configurations by combining linearly polarized TEM_{10} and TEM_{01} modes; (a) Azimuthally polarized beam (b) radially polarized beam (Rurimo, 2006).

Laser beams with polarization order number +1 are nowadays enjoying a resurgence of interest as new applications emerge and less cumbersome methods of generating them evolve. Basically, different types of experimental setups have been developed to generate these beams as described by various authors. Depending on whether the generation methods involve amplifying media, these methods can be categorized as active or passive (Zhan, 2009). Typically, active methods involve the use of laser intracavity devices that force the laser to oscillate in CV modes (Kozawa & Sato, 2005; Moser *et al.*, 2006).

One of the earliest experiments utilized an intracavity axial birefringent component (Pohl, 1972). Pohl, in his setup placed a calcite crystal in a telescope setup with its crystal axis parallel to the optical axis of the cavity. Because of double refraction, the *s* and *p* polarized components experienced slightly different magnifications. With a central stop and aperture, one polarization was discriminated more because of higher losses. The cylindrical symmetry of the entire system ensured that the oscillation mode had

cylindrical polarization symmetry. Since calcite is negatively birefringent, azimuthal polarization was generated directly in his setup whereas radial polarization was generated with optical active materials that rotated the electric field by 90^0 degrees. Although this Q-switched ruby laser was one of the pioneer works for the generation of a laser beam with cylindrically symmetric polarization, the cavity was somewhat complicated for alignment. It is important to have the optical axis of the lasing medium aligned with the optical axis of the resonator if the laser medium is also anisotropic (Zhan & Leger, 2002).

On the other hand, thermally induced birefringence of an isotropic Nd:YAG crystal was ingeniously used for the generation of a radially or azimuthally polarized beam (Moshe *et al.,* 2007). However, this method could only be applied under a strong pumping condition, thus a simple method for generating a radially polarized beam in low and middle output power ranges with isotropic laser media was required.

A method that could readily be applied to laser systems with an isotropic laser medium was demonstrated by Kozawa *et al.,* (2007). They demonstrated the generation of a radially polarized beam by simply inserting an undoped *c*-cut YVO_4 crystal into an Nd:YAG laser cavity. Due to the cylindrically symmetric and positive birefringence of the YVO_4 crystal, the stability limit of the cavity length was extended for a radially polarized beam compared to an azimuthally polarized one. By adjusting the cavity length, a radially polarized beam with an output power up to 1W was obtained. In addition, they re-arranged the cavity design to generate a higher-order transverse mode.

Besides axial birefringence, axial intracavity dichroism created with Brewster angle reflectors were also utilized to provide polarization mode selection (Kozawa *et al.,* 2005). The authors designed and fabricated a Brewster optical element that consisted of convex and concave conical prisms to generate a radially polarized laser beam. The lateral surface of the convex conical prism was coated with a dielectric multilayer (SiO_2 and Ta_2O_5) to enhance polarization selectivity. By combining the two prisms they

obtained a conical Brewster prism without beam divergence owing to refraction. A radially polarized laser mode was generated when this prism was used inside a Nd:YAG laser cavity. From a viewpoint of practical use, this conical Brewster prism was considered a suitable optical element for generation of a radially polarized beam because of its simple structure, high stability and reliability, possibility of pulsed operation, and high output power.

The use of simple binary diffraction grating has as well been utilized for the intracavity generation of radial polarization with high efficiency and simultaneously high polarization purity (Moser *et al.,* 2006). With this technique, a sealed off CO_2 laser tube was used as the gain medium.

Passive methods have also been used to generate beams with Polarization order number +1 outside the laser cavity (Oron *et al.,* 2000; Neil *et al.,* 2002; Passily *et al.,* 2005; Maurer *et al.,* 2007; Zhan, 2009). In general, these methods convert spatially homogeneous polarizations such as linear and circular polarizations into spatially inhomogeneous CV polarizations. Consequently, devices with spatially variant polarization properties are normally required. For example, axial birefringence and dichroism have been applied to generate CV beam outside the laser cavity (Zhan, 2009).

In addition, interferometric methods have also been used to generate radially polarized beams in free space (Tidwell *et al.*, 1990; Scully & Zubairy, 1991; Stalder & Schadt, 1996; Niziev *et al.,* 2006). In their works, two interferometric techniques for converting a linearly polarized laser beam into a radially polarized beam with uniform azimuthal intensity are described. These techniques are based on the linear combination of orthogonally polarized beams, which have tailored intensity and phase profiles. Linearly polarized beams with intensity profiles tailored using a modified laser or an apodization filter are combined in separate experiments to produce radially polarized light (Tidwell *et al.,* 1990).

Another scheme for converting the polarization of a laser beam based on a modified Sagnac interferometer is discussed in Niziev *et al.,* (2006). The modified Sagnac interferometer includes standard optical components such as; a displacement polarizing beam splitter, an angle reflector and a Dove prism. The radially polarized beams, obtained with the help of the developed scheme, allows the generation of a longitudinally polarized electric field by sharp focusing. The phase correction of radially polarized modes of higher orders led to an increased longitudinal field in the focus of the beam.

Spatially variant polarization rotation can also be utilized to produce CV beams. In this case, linearly polarized light is typically used as input and then locally rotated to the desired spatial polarization pattern (Zhan, 2009). One of the methods involves a liquid crystal (LC) cell operated in a metastable state (Quabis *et al.,* 2005; Rurimo, 2006; Maekawa & Uesaka, 2008). The LC cell is made of one unidirectional and one circularly rubbed alignment structure on two opposing glass plates. The space separating the plates is filled with a nematic liquid crystal. Transparent tin oxide electrodes are attached to the glass plates and are used to supply an electric field which causes the alignment of the liquid crystal molecules. By changing the orientation of the incident beam polarization, the LC cell output can easily switch from radial to azimuthal polarization and vice versa. The main disadvantage with this method is its temporal instability with regard to the orientation of the liquid-crystal molecules (Rurimo, 2006).

Another suitable choice is the use of a segmented half waveplates polarization converter which is made from segments cut from a commercial half wave plate (Quabis *et al*., 2005; Machavariani *et al.,* 2007; Maekawa & Uesaka, 2008). The joining together of the segments is done in such a way that their fast axes points in different directions allowing the local rotation of the electric field vectors of an incident linearly polarized beam. The conversion efficiency of such a converter is dependent on the number of the segments used (Quabis *et al*., 2005).

Other methods reported include; (i) Use of few-mode fibers as demonstrated by Volpe and Petrov, (2004). The authors demonstrated both theoretically and experimentally that the excitation of a few-mode fiber with a first-order LG beam is an efficient method for producing high quality CV beams. (ii) The use of leaky mirrorless laser has been exploited as described in (Ellenbogen *et al.,* 2012). Using this method, both radially and azimuthally polarized beams were generated by leaky emission from photo-excited molecules embedded in slab-optical-waveguides which are formed on thin metal films on glass.

A number of applications have favored radially and azimuthally polarized beams because of the unique characteristics in their focal regions when focused using a high NA focusing objective. For instance, an optimized polarization distribution improves the absorption of the laser radiation in laser machining and therefore significantly influences the overall efficiency (Niziev & Nesterov, 1999; Ahmed *et al*., 2009; Steen & Mazumder, 2010; Krishnan & Tan, 2012). Laser machining is one of the fastest growing processes in industrial manufacturing and is being used widely in metal cutting, drilling and welding. Compared with conventional tools, it offers significant advantages in productivity, machining precision, part quality, material utilization and flexibility. Up to 50% higher cutting efficiency is obtained in the experiments with radial polarization in comparison to circular polarization (Ahmed *et al.,* 2009). Additionally, the roughness of the cut edge is shown to reduce by 50% with radial polarization which is a significant quality improvement. In micro-drilling experiments, azimuthally or radially polarized beams are reported to significantly enhance the drilling efficiency (Niziev & Nesterov, 1999; Ahmed *et al*., 2009; Steen & Mazumder, 2010).

Another interesting area of application is the acceleration of electrons (Romea & Kimura, 1990; Scully & Zubairy, 1991; Maekawa & Uesaka, 2008). This involves the transfer of light energy to an electron beam via the inverse Cherenkov Effect. In this process, a radially polarized laser beam is focused by an axicon lens to produce an annular set of plane waves that subtends an angle θ_c (Cherenkov angle) along the optical

axis. Further, for a radially polarized input field, the transverse electric field component cancels out almost entirely on-axis. The longitudinal electric field component is the significant component in the acceleration process.

The focusing properties of radially polarized beams have interesting applications in optical trapping (Dorn *et al.*, 2003; Zhan, 2004; Kozawa & Sato, 2010). The authors have demonstrated that optical tweezers using radial polarization can stably trap metallic particles in 3-dimensions. The extremely strong axial component of a highly focused radially polarized beam provides a large gradient force. Owing to the spatial separation of the gradient force and scattering/absorption forces, a stable 3D optical trap for metallic particles can be formed (Zhan, 2009).

1.3 Cellophane sheet as a birefringent material

Cellophane is a thin, flexible and transparent organic polymeric material made from wood pulp. It is fabricated by extruding a viscose solution through a dye into a bath of dilute sulfuric acid and sodium sulfate. As a result of differential strains between the longitudinal and transverse directions of the protrusion, the refractive index of the light polarized parallel to the slit is smaller than that of the light polarized perpendicular to the slit. This means the phase velocity of the light wave polarized parallel to the slit (fast axis) is faster than that of the wave polarized perpendicular to the slit (slow axis). Thus, optically the cellophane sheet is birefringent and the directions of fast and slow axes are perpendicular to each other. It is widely used as wrappers and in packaging food and merchandize since it is impermeable to gases, grease, or bacteria.

A cellophane sheet is a good choice of a birefringent material since its fibers lie preferentially in a certain direction. It is approximately 25 μm thick and can be cut to almost any desirable size with ease. It has been experimentally verified that it possesses properties of a wide wavelength spectrum half waveplate (Ortiz *et al.*, 2001). As an example of its applications, cellophane displays superior performance when used for rotating the direction of polarization of light than a commercially available half-wave plate with a specified wavelength (Iizuka, 2003; Rurimo, 2006). An ordinary screen of a

laptop is converted into a 3D display using the cellophane birefringence (Iizuka, 2012). As such, the author fabricated a complementary cellophane optic gate which was used to convert an ordinary iPad into a 3D display. As well, the birefringence property of transparent, colorless stretched cellophane has been used in the production of a variety of colors (Edwards & Langley, 1981) among other applications. Additionally, it has been shown that the price per square centimeter of the cellophane sheet is about 1/3500 that of a commercially available half-wave plate (Iizuka, 2012). Thus, the use of a cellophane sheet in generating laser beams of polarization order number +1 is evidently cheap and reliable.

In this research, several cellophane sheets from different manufacturers were tested for the property of birefringence. Some did not posses any birefringence at all while others possessed insufficient birefringence at the wavelength of 632.8 nm.

1.4 Retardation phase plates

The basic optical elements for polarization measurements are the retardation phase plates and linear polarizer (Berry *et al.*, 1977). The retardation phase plates operate by imparting unequal phase shifts to x- and y- polarized components of an incident light beam. Since the x- and y- polarizations travel with different velocities, their phases change at a different rate as the light passes through the plate. Inside the plate, the phase difference (φ) between x- and y- vibrations is proportional to the depth in the substance. This is the operation mode of the standard retardation phase plates. The phase difference (φ) between the two polarization components on emergence is given by;

$$\varphi = \frac{2\pi}{\lambda}\left(\eta_x - \eta_y\right)d \qquad 1.1$$

Where λ is the wavelength of the light source, η_x and η_y is the refractive indices of the slow and fast axis respectively and d is the depth of the plate.

The most commonly made retardation phase plates are the half-waveplate (HWP) and quarter-waveplate (QWP). The HWP introduces a phase difference of 180^0 degrees (π)

whereas a QWP results in a value of 90^0 degrees $(\pi/2)$ as phase difference. When a linearly polarized beam is passing through a HWP, it emerges as a linearly polarized beam but its polarization plane is rotated with respect to the polarization plane of the input beam. The rotation of the polarization plane corresponds to twice the angle between the input polarization and the waveplate axis. In the case of QWP, applying a linearly polarized beam with the polarization plane aligned at 45 degrees to the optical axis of the waveplate, the output beam will be circularly polarized. Similarly, when applying a circularly polarized beam through a QWP, the output beam will be linearly polarized (Hecht, 2001).

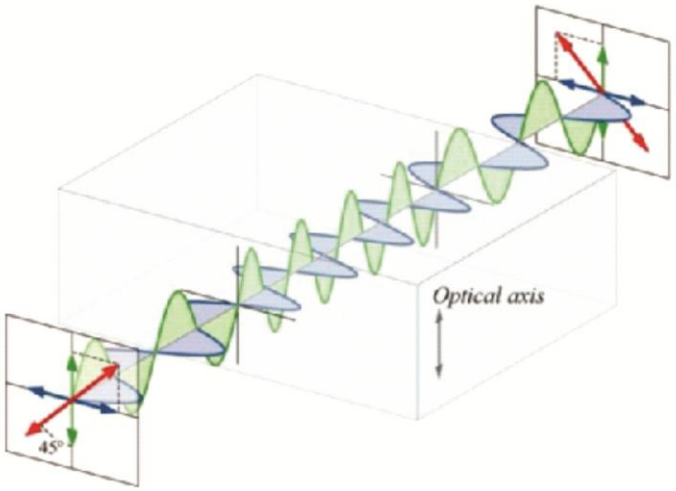

Figure 1.2: Behavior of light through a half-wave plate. The beam is resolved into green and blue components defining the fast and slow axis respectively (Hecht, 2001).

Linearly polarized light entering a waveplate can be resolved into two waves, parallel (green) and perpendicular (blue) to the optical axis of the wave plate. At the far side of the plate, the parallel wave is exactly half of a wavelength delayed relative to the perpendicular wave, and the resulting combination (red) is orthogonally polarized compared to its entrance state.

On the other hand, a polarizer has the useful property that it transmits light that is linearly polarized parallel to the axis of the polarizer with very little absorption, but light polarized in a direction perpendicular to the axis of the polarizer is strongly absorbed. When unpolarized light is passed through a polarizer, only that part of the unpolarized beam which is oscillating parallel to the axis of the polarizer gets through, so that the transmitted beam is linearly polarized. The same property of a polarizer is useful in detecting the direction of polarization of a linearly polarized beam, or in determining whether a beam is actually linearly polarized or not.

1.5 Stokes polarization parameters

The state of polarization of a light beam can be characterized in terms of four intensity parameters referred to as the Stokes polarization parameters named after George Gabriel Stokes (Berry *et al.,* 1977; Schaefer *et al.,* 2007). The Stokes polarization parameters are widely used to describe the polarization behavior of an optical beam primarily due to the fact that the polarization ellipse, which is an amplitude description of polarized light, is not directly accessible (experimentally) to measurement. The polarization ellipse and its associated orientation and ellipticity angles have been shown to be directly related to the Stokes polarization parameters (Born & Wolf, 1999).

Although several measurement methods can be used to determine the Stokes parameters, the Rotating quarter waveplate technique was chosen for this research. This is because of its ease in implementation and still achieves the purpose of this research. In addition, this technique avoids the limitations of the classical method, and allows for a curve fitting algorithm to be used to automatically determine the Stokes parameters (Schaefer *et al.,* 2007).

1.5.1 The polarization ellipse and the Stokes polarization parameters

The Stokes polarization parameters describe not only completely polarized light but partially polarized light and unpolarized light as well. Principally, the electric field of an optical beam (paraxial approximation or plane wave) consists of two independent

orthogonal components, $E_x(z,t)$ and $E_y(z,t)$, that have different amplitudes and phases. The direction of propagation is in the z-direction (Hecht, 2001). The equations that describe this behavior are;

$$E_x(z,t) = E_{0x}Cos(\omega t - kz + \delta_x) \quad 1.2$$

$$E_y(z,t) = E_{0y}Cos(\omega t - kz + \delta_y) \quad 1.3$$

Where t represents the time, E_{0x} and E_{0y} are the maximum amplitudes of the optical field, $\omega = 2\pi\vartheta$ is the angular frequency, ϑ is the frequency of oscillation, $k = 2\pi/\lambda$ is the wave number, and δ_x and δ_y are the phase constants. The term $(\omega t - kz)$ describes the propagation of the wave and is called the propagator. At optical frequencies the duration for a single wave to repeat its oscillation is of the order of 10^{-15}s (Schaefer *et al.,* 2007). This time interval is for all practical purposes immeasurable and so the frequency of oscillation cannot be directly observed or measured.

A useful visual representation of the polarization behavior of the optical beam can be obtained by eliminating the propagator in equation above between equations 1.2 and 1.3 yielding;

$$\frac{E_x(z,t)^2}{E_{0x}^2} + \frac{E_y(z,t)^2}{E_{0y}^2} - \frac{2E_x(z,t)E_y(z,t)}{E_{0x}E_{0y}}Cos\delta = \sin^2\delta, \text{ where } \delta = \delta_y - \delta_x \quad 1.4$$

Equation 1.4 describes the polarization ellipse. However, the ellipse can neither be observed nor measured. To determine the parameters of the polarization ellipse (that can be observed), equation 1.4 must be transformed into the intensity (observable) domain (Collet, 1968). This transformation can be done by taking a time average of the above equation yielding the relation;

$$S_0^2 = S_1^2 + S_2^2 + S_3^2 \quad 1.5$$

Where,

$$S_0 = E_{0x}^2 + E_{0y}^2 \quad 1.6$$

$$S_1 = E_{0x}^2 - E_{0y}^2 \quad 1.7$$

$$S_2 = 2E_{0x}E_{0y}\cos\delta \quad 1.8$$

$$S_3 = 2E_{0x}E_{0y}\sin\delta \quad 1.9$$

These four equations define the four Stokes polarization parameters. They are described in terms of intensities (amplitudes squared) and thus can be measured. The parameter S_0 describes the total intensity of the optical field, S_1 describes the linear polarization along the horizontal and vertical axis, S_2 describes the linear polarization along the diagonals, and the fourth parameter S_3 characterizes the extent to which the beam is either right or left circularly polarized light. The Stokes parameters can be arranged as the elements of a 4x1 matrix as;

$$S = \begin{pmatrix} S_0 \\ S_1 \\ S_2 \\ S_3 \end{pmatrix}.$$

The polarization state is completely determined by the three ratios S_1/S_0, S_2/S_0, S_3/S_0, referred to as relative Stokes parameters. They have possible values between -1 and +1 (Berry *et al.*, 1977).

1.5.2 The Rotating Quarter Waveplate measurement technique

This technique overcomes the drawbacks of the Classical measurement technique which for instance: i) requires that the transmission axis of the linear polarizer be aligned as accurately as possible to the required angles, ii) that in the final measurement the quarter waveplate must be inserted and aligned which in turn absorbs light. This introduces a systematic error to the Stokes parameters (Born & Wolf, 1999). The chances of error in the classical technique are also very high since only four data points are measured.

Figure 1.3 shows the measurement configuration with the polarizing elements that generate the Stokes parameters to be measured. The quarter waveplate in this setup is rotatable through an angle θ; it is then followed by a fixed linear polarizer whose transmission axis is fixed in the direction of the $x-$axis.

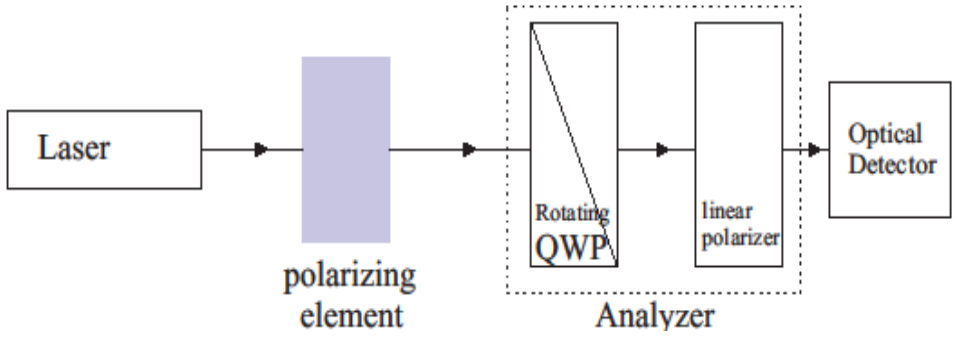

Figure 1.3: Setup for the rotating quarter waveplate technique of measuring Stokes polarization parameters. The figure shows the polarizing elements that generate the Stokes parameters to be measured. The QWP can be rotated while the linear polarizer is fixed.

The intensity of the beam measured by the detector is dependent on the angle of the QWP as in equation 1.10 (Collet, 1993);

$$I(\theta)=\frac{1}{2}\left(S_0+S_1\cos^2 2\theta+S_2\cos 2\theta\sin 2\theta+S_3\sin 2\theta\right) \qquad 1.10$$

Equation 1.10 corresponds to the optical beam that emerges from the polarizing element(s). The squared and product terms in the equation can be rewritten by using the trigonometric half-angle formula to yield equation 1.11 (Collet, 1993);

$$I(\theta) = \frac{1}{2}\left(A + B\sin 2\theta + C\cos 4\theta + D\sin 4\theta\right) \qquad 1.11$$

Where,

$$A = S_0 + \frac{S_1}{2}; B = S_3; C = \frac{S_1}{2}; D = \frac{S_2}{2}.$$

The stokes parameters are thus found to be;

$$S_0 = A - C,$$
$$S_1 = 2C,$$
$$S_2 = 2D, and$$
$$S_3 = B.$$

Because intensities are measured for discrete angles, equation 1.11 is re-written as;

$$I_n = \frac{1}{2}\left(A + B\sin 2\theta_n + C\cos 4\theta_n + D\sin 4\theta_n\right), \quad n = 1,2,....., N \text{ for } N \geq 8 \qquad 1.12$$

Where N is an even number. The coefficients A, B, C, and D are determined using familiar methods from Fourier analysis (Lee & Messerschmidt, 1994) and are given by;

$$A = \frac{2}{N}\sum_{n=1}^{N} I_n, B = \frac{4}{N}\sum_{n=1}^{N} I_n \sin 2\theta_n \qquad 1.13\ (a)$$

$$C = \frac{4}{N}\sum_{n=1}^{N} I_n \cos 4\theta_n; D = \frac{4}{N}\sum_{n=1}^{N} I_n \sin 4\theta_n \qquad 1.13\ (b)$$

In these two equations, the intervals are equal and are given by;

$$\theta_{n+1} - \theta_n = \frac{180^0}{N} \qquad 1.14$$

Using the quarter waveplate technique, the QWP needs to be rotated through 180^0, with at least eight steps to obtain a complete set of the Stokes parameters (Schaefer *et al.*, 2007).

1.6 Laser Cutting

Most laser cutting is carried out using CO_2 or Nd:YAG lasers. The general principles of cutting are similar for both types of laser although CO_2 lasers dominate the market. The reason is that CO_2 lasers offer a cheaper production route and also have the advantage that they can cut a wider range of materials from metals to polymers and wood (Powell & Kaplan, 2004).

The CO_2 laser systems are computer-controlled and can be used for laser marking, engraving and cutting operations. These laser processing systems transform images or drawings on a computer screen into real items made out of a variety of materials such as wood, plastic, fabric, paper, glass, leather, stone, ceramic, rubber among many others. The system is directly compatible with popular Windows based Computer Aided Design (CAD) and graphics programs, so there is no need for proprietary conversion software in order to engrave graphic images and logos. It is fitted with;

i. **An Auto Focus** which **s**ets the work table to proper height for laser processing. This simplifies the setup process by assuring proper in-focus position for items placed on the work table. This also eliminates wasted material common when one forgets to focus with a manual focus system.
ii. **Honeycomb Cutting Table** which supports the materials being laser cut and provides some vacuum hold down. This minimizes burning of the back side of materials being cut all the way through by supporting materials above the reflective work table in the machine. The honeycomb design supports even small cut parts. The cutting table is designed to draw air through it to remove smoke

and cutting vapors as they are generated which aids in keeping the cut parts and the machine cleaner. The table has ruler guides to aid in positioning materials.

iii. **Red Laser Pointer-** This is a visible red beam used as the material positioning tool. It simplifies and speeds setup by verifying exact position of odd shaped items on the work table. The position on the work table that the beam points to is displayed in X-Y coordinates to allow proper job setup. The beam can also be turned on in a simulated machine run to point to where the processing laser beam will be during an actual production run.

The basic mechanism of laser cutting is extremely simple and can be summarized as follows:

1. A high intensity beam of infrared light is generated by a laser.
2. This beam is focused onto the surface of the work piece by means of a lens.
3. The focused beam heats the material and establishes a much localized melt (generally smaller than 0.5 mm diameter) throughout the depth of the sheet.
4. The molten material is ejected from the area by pressurized gas jet acting coaxially with the laser beam as shown in figure 1.4.
5. This localized area of material removal is moved across the surface of the sheet thus generating a cut. Movement is achieved by manipulation of the focused laser spot (by CNC mirrors) or by mechanically moving the sheet on a CNC X-Y table. 'Hybrid' systems are also available where the material is moved in one axis and the laser spot moved in the other. Fully robotic systems are available for profiling three dimensional shapes.

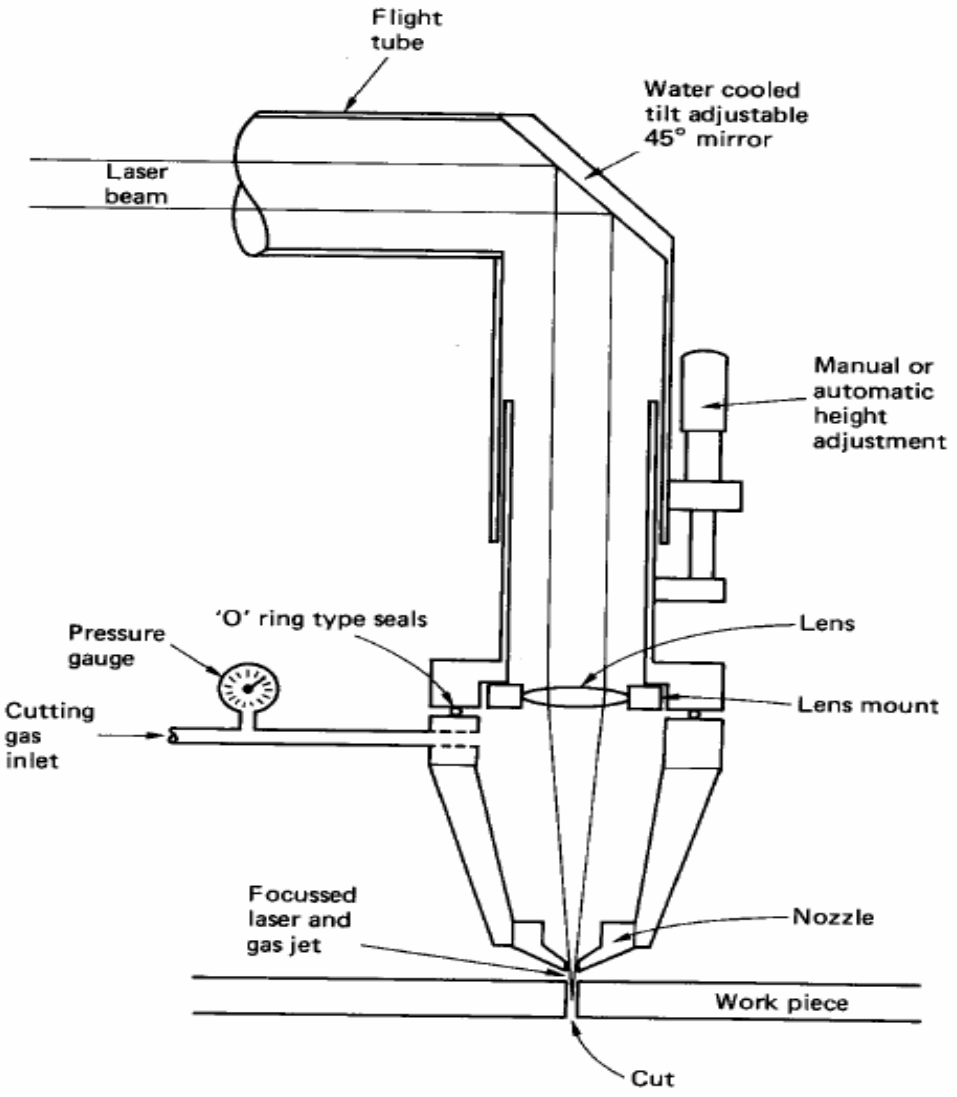

Figure 1.4: A schematic of laser cutting (Powell & Kaplan, 2004). The lens mount or the nozzle (or both) can be adjusted from left to right or into and out of the plane of the sketch. This allows for centralization of the focused beam with the nozzle. The vertical distance between the nozzle and the lens can also be adjusted.

1.7 Statement of the problem

Numerous techniques for obtaining beams with polarization order +1, that could potentially have higher efficiencies, have been investigated in the past, but all have had short-comings. Some of these techniques involve difficult and impractical refractive index matching techniques while in others, the polarization purity of the resultant either radially or an azimuthally polarized beam is relatively poor. Additionally, some of these methods are cumbersome, very expensive and characterized by relatively low light throughput efficiency. To address these challenges, this research came in handy to provide a simple, reliable, cost effective and practical method of obtaining both radially and azimuthally polarized laser beams of high quality.

1.8 Justification

The success of this research is a major step forward for upcoming institutions in Optics and especially in the third world. The approach presented in this thesis is simple and can be readily implemented. Additionally, it has the advantage of being cheap, reliable and allowing existing lasers to be used.

1.9 Objectives

1.9.1 General Objective

To design and implement an experimental setup to generate either radially or azimuthally polarized beams

1.9.2 Specific Objectives

1. To determine the birefringence property and establish the axes of a cellophane sheet
2. To fabricate a polarization mask for the generation of beams with either radial or azimuthal polarization state.
3. To analyze the polarization state of the generated beams

CHAPTER TWO

2.0 MATERIALS AND METHODS

2.1 Introduction

This chapter contains the experimental procedure for cellophane sheet analysis, generation of beams with polarization order number +1 and other related experiments. A frequency stabilized He-Ne laser operating at a wavelength λ = 632.8 nm and manufactured by Thorlabs Inc., was used as light source. The laser beam was spatially filtered by transmitting it through a Polarization Maintaining Fiber (PMF) and afterwards collimated by use of a Microscope Objective (MO) with a magnification X10, and NA of 0.25 supplied by CVI Melles Griot. The beam was magnified to a larger diameter to ensure it covered a larger portion of the cellophane sheet and thereby minimize the effect of a non-perfect central area of the polarization mask. It was then collimated using a doublet lens.

A CO_2 laser engraving/cutting machine (Epilog Helix 24) was used to cut the cellophane segments at the University of Erlangen, Germany. A motorized rotation stage/mount (PRM1/MZ8, Thorlabs Inc.) controlled via a software interface was used for mounting and for precise angular adjustment of the test cellophane samples, the HWP and the QWP. A digital handheld laser power meter (PM100D, Thorlabs Inc.) was used to record power fluctuations of the laser source. A DMK 31BU03- CCD camera with a pixel resolution of 1024x768, interfaced to a desktop computer via USB 2.0 was used to capture all the image patterns. Finally, the analysis of the data was done using Origin pro, Atmos fringe and MATLAB softwares.

2.2 Measurement of laser beam stability

For measuring the power stability of the He-Ne laser, the setup in figure 2.1 was arranged on an optical table. The laser beam was passed through an optical isolator (OI) which served to block unwanted back reflections into the laser cavity. It was then transmitted through a PMF for spatial filtering. The diverging beam behind the PMF was collimated by a MO. It was then split into two parts by inserting a non-polarizing beam

splitter cube (with a 50:50 split ratio) in the beam path. A photodiode sensor connected to a power meter and a CCD camera connected to a computer were placed in the reflected and transmitted parts of the beam respectively as shown in figure 2.1. A neutral density filter (DF) with a transmission of 1% was placed before the beam splitter to prevent oversaturation of the detectors.

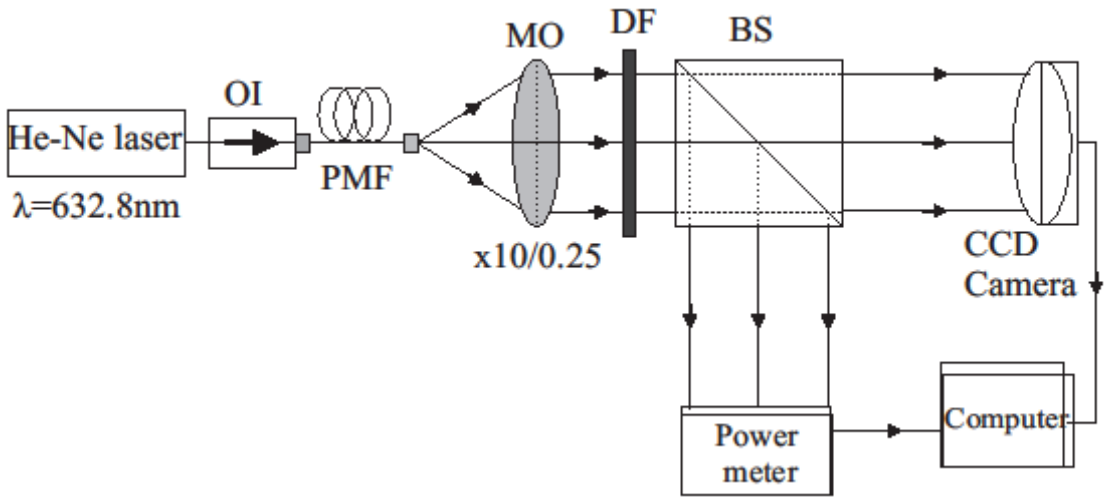

Figure 2.1: Optical setup for measuring the power stability of the He-Ne laser. OI is the optical isolator; PMF is the polarization maintaining fiber used for spatial filtering while MO is the microscope objective utilized for collimation. DF is a neutral density filter and BS is the beam splitter.

The power meter was used to measure the power of the reflected part of the beam which was utilized as the reference signal while the CCD camera captured images of the transmitted part of the beam. Using MATLAB software, intensity of the respective images captured was evaluated. The recording of power and the images occurred simultaneously, as displayed in appendix 1.

2.3 Spatial filter and beam expansion

The diameter of the collimated beam behind the MO was further expanded in order to cover a bigger portion of the cellophane sheet and thereby to minimize the effect of a non-perfect central area of the fabricated polarization mask. For this purpose, a telescopic configuration shown in figure 2.2 was used. It comprised a pinhole (PH) and two doublet lenses with focal lengths of 80 mm and 160 mm respectively. The pinhole of diameter 20 µm was included to reduce aberrations caused by the non-perfect end-face of the PMF.

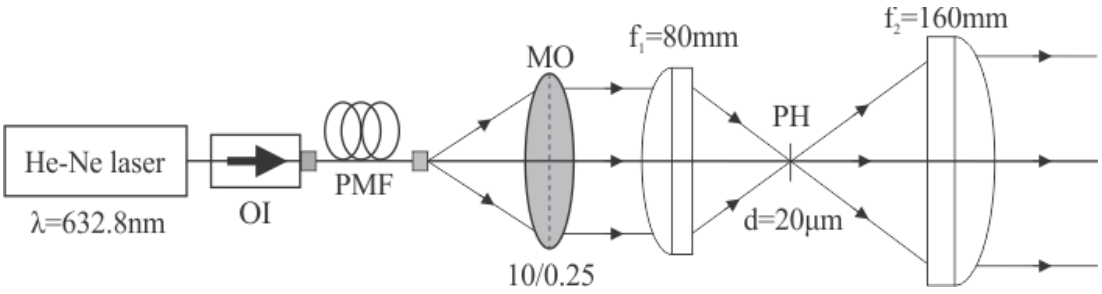

Figure 2.2: Experimental setup used to spatially filter, collimate and magnify the already collimated laser beam.

The lens with the focal length f_1 = 80 mm was placed in the beam path to focus the already collimated beam. The second lens with focal length f_2 = 160 mm was used to collimate the diverging beam. In between, a pinhole with diameter d = 20 µm was introduced to further reduce aberrations due to MO and the first lens. All elements were carefully aligned until a bright, expanded and collimated beam was obtained with few or no diffraction rings surrounding it.

2.4 Identifying a Cellophane sheet with birefringence property

2.4.1 Polariscope test

The schematic setup shown in figure 2.3 was used to investigate and identify the cellophane sheet(s) exhibiting birefringence properties. The setup is composed of a He-Ne laser, a non-polarizing BS, 2-linear polarizers (Lp_1 and Lp_2), each with defined transmission axes, power meter and a CCD camera, both interfaced to a desktop

computer. The linearly polarized, spatially filtered and collimated light beam from a He-Ne Laser (as described in Section 2.3) was passed through the BS. The reflected part of the beam was coupled to a power meter. This beam was used as the reference signal in a normalization process which eliminates any power fluctuations from the measured data due to the optical setup. The transmitted part of the beam was guided through the optical elements.

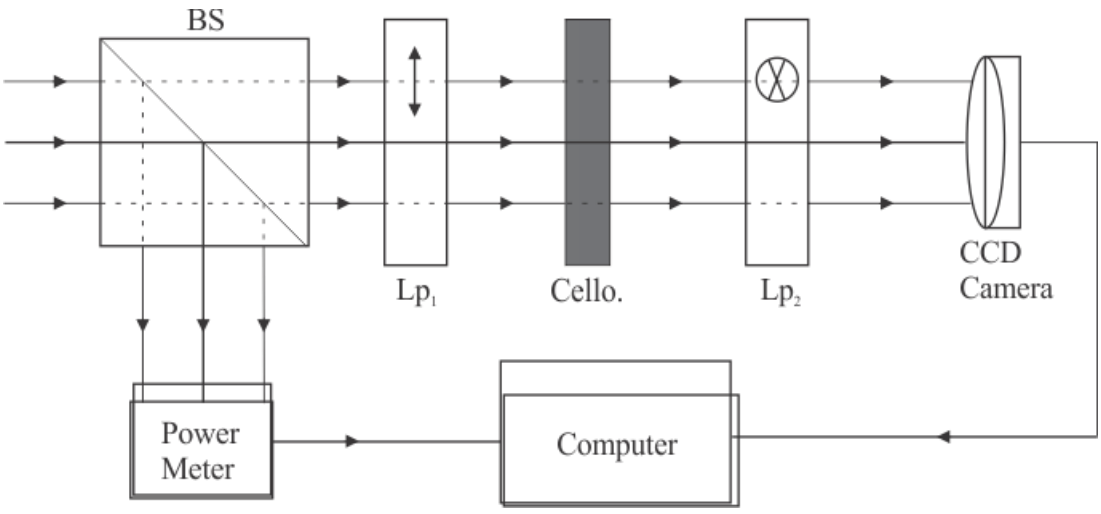

Figure 2.3: Experimental setup used to investigate the birefringence property of the cellophane sheet(s). Lp_1 and Lp_2 are linear polarizers whose transmission axes are perpendicular to each other. Cello. is the cellophane sample being tested.

The polarizer Lp_1 gives the polarization direction of the input laser beam while the polarizer Lp_2 serves to detect any polarization rotation the cellophane may have caused on the light beam passing through it. The axes of the polarizers were set perpendicular to each other. The cellophane sample was mounted on a motorized rotation stage which was computer controlled. It was introduced between the polarizers and rotated in steps of 5 degrees about the beam axis. A CCD camera interfaced with a computer was used to observe the behavior of the light beam behind the second polarizer by capturing images with each rotation step. Various cellophane sheet samples from flower wrappings and gift baskets were tested. The respective data values recorded are displayed in appendix

2. The sheet that displayed the largest polarization rotation as depicted from the light intensity transmitted by Lp_2 was selected.

2.4.2 Determination of the fast or slow axis of cellophane

It was necessary to make an absolute determination of the fast or slow axes of the cellophane sample. This would ensure a proper orientation of the cellophane sheet in the fabrication of the polarization mask. To make this determination, another experiment as described in section 2.4.1 was performed using a commercial HWP with known fast axes. Results obtained for both cellophane and commercial HWP were tabulated (as shown in appendix 2), analyzed and are presented in section 3.3.

2.4.3 Measuring the Stokes polarization parameters for the cellophane sheet

To describe the polarization properties of the cellophane sheet, the Stokes polarization parameters were measured with the setup presented in figure 2.4. The cellophane sheet was mounted with its fast axis at an angle of 45 degrees relative to the incoming polarization axis. The QWP was mounted on a motorized rotation stage which was computer controlled. It was inserted in the beam path between the cellophane sheet and a linear polarizer whose transmission axis was fixed along the direction of the laser beam polarization. Images of the beam after passing through the linear polarizer Lp_2 were captured using a CCD camera interfaced to a desktop computer. These images were analyzed and their respective intensities evaluated using MATLAB software.

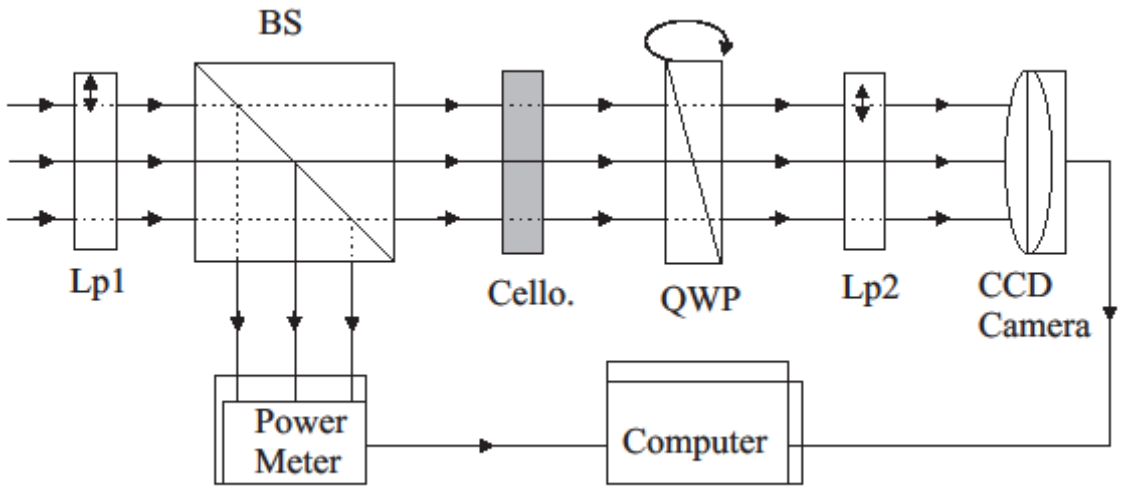

Figure 2.4: Experimental setup for measuring the Stokes polarization parameters of the beam after passing through the cellophane sheet. The cellophane was fixed in the beam path and oriented with its fast axis at an angle of 45 degrees with respect to the incoming polarization. The QWP was rotatable while the transmission axis of the linear polarizer was fixed.

2.5 Design and fabrication of the Polarization Mask

The artwork of the typical segments (as illustrated in figure 2.5) was first created using CorelDraw graphic software. The segments were drawn such that each quadrant had its fast axis oriented in an appropriate direction. For ease of identification and positioning, the segments were drawn with different patterns and extensions or flaps to aid in holding when joining them together. With the prepared artwork on the computer, the cellophane sheet was placed on the work surface of the CO_2 laser engraving/cutting machine (shown in figure 2.6) for cutting of the segments. The cellophane sheet cut had been verified for birefringence properties and its axes determined using the procedure described in section 2.4.2.

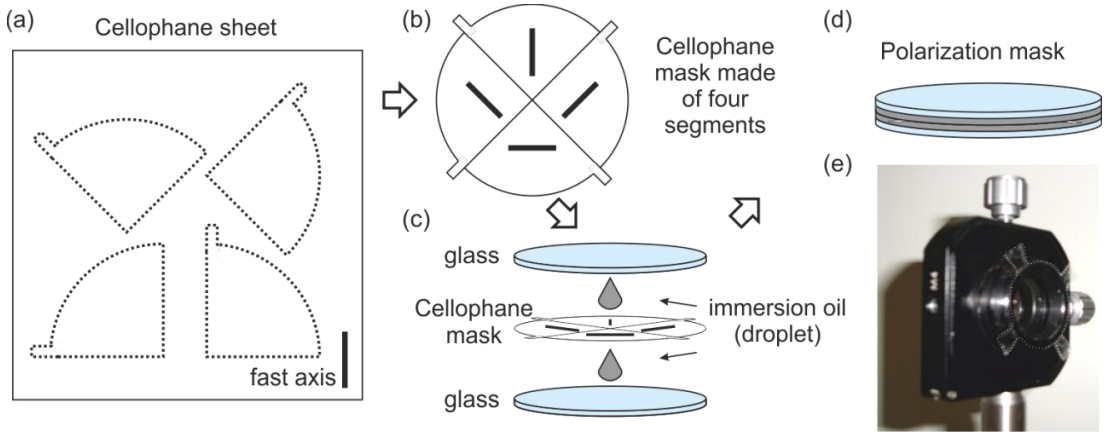

Figure 2.5: (a) Cutting template for the Cellophane. (b) The four Cellophane segments assembled to form the desired polarization mask. (c) The polarization mask is fixed between two microscope cover slips and immersion oil is inserted. (d) Sketch and (e) an image of the fabricated polarization mask mounted on a lens holder.

In order to complete the polarization mask, the four segments were joined together using immersion oil. The joined segments were sandwiched between two microscope cover slips (glass plates) for support.

Figure 2.6 shows a photograph of the CO_2 laser engraving/cutting machine used in the cutting of cellophane into the respective segments.

Figure 2.6: Photographs of a section of the CO_2 laser engraving/cutting machine (Epilog Helix 24) used to cut the cellophane segments at the technical science laboratory, University of Erlangen, Germany.

2.6 Generation of either radially or azimuthally polarized beams

The setup for the conversion of a linearly polarized Gaussian to a radially or azimuthally polarized beam was aligned as shown in figure 2.7. A photograph of this section of the setup with some optical elements mounted on an optical table is appended in appendix 4. The linearly polarized fundamental Gaussian mode of a frequency stabilized He-Ne laser (wavelength λ = 632.8 nm) was spatially filtered, expanded and collimated. It was passed through linear polarizer, Lp_1 which served to define its polarization as either horizontal or vertical. A HWP was inserted in the beam path before the polarization mask to rotate the polarization of the input linearly polarized beam such that either radial or azimuthal beams were generated. Subsequently, the beam was passed through the polarization mask which converted the Gaussian beam into a pseudo-doughnut beam. An image of the beam was captured using a CCD camera positioned at point A in figure 2.7 and is presented in figure 3.8 (a).

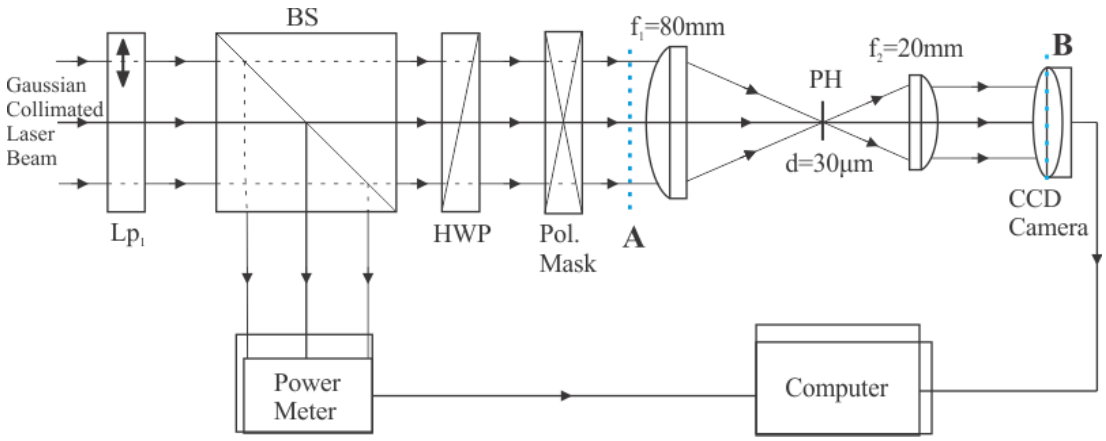

Figure 2.7: Experimental setup for the generation of either radially or azimuthally polarized beams. An incoming linearly polarized Gaussian beam was passed through the fabricated polarization mask. Image patterns of the beam behind the polarization mask were captured using a CCD image sensor positioned at Point A, and then at point B (after spatial filtering). The spatial filtering was achieved with pinhole of diameter d = 30µm and two doublet lenses of focal length 80 mm and 20 mm respectively.

To achieve high mode purity of the fundamental cylindrically polarized mode, the higher order modes are filtered out utilizing a spatial filter. The spatial filter comprised of two doublet lenses and a pinhole of diameter 30 µm as shown in figure 2.7. With the second lens after the pinhole, the beam was collimated and its image pattern captured using a CCD camera.

2.7 Analysis of the polarization state of the generated beams

2.7.1 Using a rotating linear polarizer

To verify the polarization state of the beam generated using the polarization mask, the setup described in figure 2.7 was modified. A rotatable linear polarizer with known transmission axis was introduced in the beam path after collimation. A CCD camera interfaced with a computer was used to capture the beam patterns or lobes with each rotation of the linear polarizer. The image patterns captured are presented in section 3.5.

2.7.2 Measuring the Stokes polarization parameters of the generated doughnut beams

The measurement configuration shown in figure 2.8 was used to determine the Stokes parameters of the generated doughnut beam. A quarter waveplate (QWP) was mounted on a motorized rotation stage. It was inserted in the beam path after the polarization mask between the collimating lens and the linear polarizer Lp_2. The transmission axis of the linear polarizer was aligned parallel to the polarization axis of the input beam.

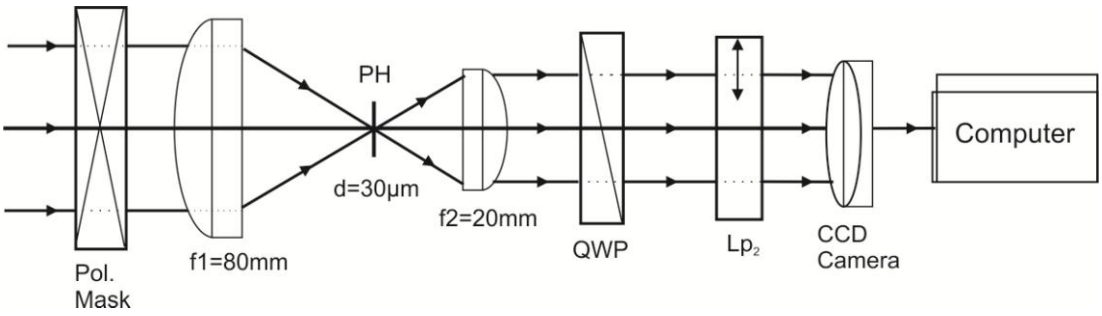

Figure 2.8: Setup for measuring the Stokes polarization parameters of the generated doughnut beam. The QWP was rotatable through an angle θ while the linear polarizer was fixed. A CCD camera interfaced with a computer was used to capture the image patterns.

The output beam (after spatial filtering) was passed through a rotatable QWP and a fixed linear polarizer. Behind the polarizer, a CCD camera was used to measure the beam profile for different angular positions of the quarter-wave plate. Using the algorithm introduced by Schaefer et al., (2007), the spatially resolved Stokes parameters were reconstructed (see figure 3.12) from sixteen different images of the beam.

CHAPTER THREE

3.0 RESULTS AND DISCUSSION

3.1 Introduction

In this chapter, results are presented and discussed with the aid of graphs and tables. The chapter starts with profiling the He-Ne laser that was used in this study in terms of its stability, and spatial intensity distribution. In particular, techniques to decrease the influence of temporal power fluctuations of the laser beam on the polarization measurements are discussed. The chapter includes a detailed analysis of the cellophane sheet tested and a comparison to the commercial half waveplate (HWP). Thereafter, the fabricated polarization mask is presented and discussed. The basic principle for the conversion of a linearly polarized Gaussian beam into a pseudo-doughnut beam using the polarization mask is presented. Images of the experimentally generated doughnut beams captured using the CCD camera are presented and discussed. Finally, results for the analysis of the polarization state of the generated doughnut beams using both the rotating linear polarizer and the Stokes measurements are presented and discussed. In addition, techniques for improving the quality of the generated modes have also been mentioned.

3.2 Stability of the experimental set-up

In research and application laboratories, it is often necessary to conduct experiments or take measurements in a vibration-free environment. However, uncontrollable sources of vibrations contribute to an unavoidable background noise. Vibration, which is commonly referred to as noise, can be categorized into: Seismic (ground) vibrations, acoustic vibrations and forces applied directly to the load on the working surface. Typically, the frequency of the vibrations ranges from 4-100Hz. Thus, to ensure a vibration-free environment, all the experiments were performed on an optical table that was pneumatically suspended. This provided a rigid base on which the optics were mounted and aligned reliably with long term stability. Additionally, it not only successfully damped the vibrations, but also isolated the experiment as a whole from

ambient background laboratory vibrations. Further, a linear setup was used because it features a high level of stability.

3.2.1 Measurements of laser intensity fluctuations

As aforementioned, the source of light was a He-Ne gas laser emitting red light at a wavelength of 632.8 nm. Due to its narrow gain bandwidth, it typically exhibits stable single-frequency operation with excellent beam quality. However, intensity fluctuations caused by either mode hoping or deviations of the fibre coupling efficiency are possible. The intensity fluctuations, commonly referred to as noise, results partly from either quantum noise which is associated with laser gain and resonator losses or technical noise sources such as excess noise of the pump source, vibrations of resonator mirrors, thermal fluctuations in the gain medium, etc.

The intensity fluctuations measured using the setup, described in Section 2.2, are shown in figure 3.1. During the experiment, the power meter recorded power whereas the CCD camera captured the images of the beam with each angular rotation. A short code was developed and interfaced to the setup such that the recording of power and capturing of the images occurred nearly simultaneously. Using MATLAB and Origin pro softwares, the images were analyzed and their respective intensity evaluated.

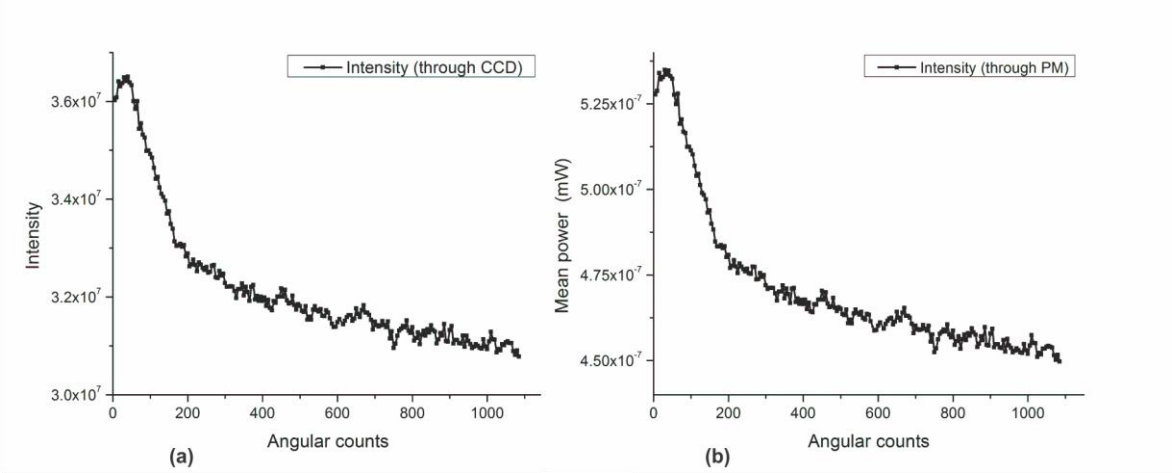

Figure 3.1: Graphs of Intensity of the beam through (a) the CCD-camera and (b) power meter plotted against the angular counts (time). Strong intensity fluctuations are evident for the transmitted and reflected parts of the beam. The angular counts are proportional to the time.

The data is taken immediately after switching on the laser. At the onset of the measurements, there is a rapid fall in the laser intensity (as shown in figure 3.1). One expects strong fluctuations as the laser warms up. Both the reflected and the transmitted parts of the beam exhibit similar intensity fluctuations as shown in figure 3.1.

Defining the percentage intensity fluctuation as the ratio of the fluctuations to the average intensity in the given time period, as shown in equation 3.1;

$$\%\ \text{Intensity Fluctuations} = \left(\frac{I_{Max} - I_{Min}}{I_{Max} + I_{Min}} \right) X\,100 \qquad 3.1$$

The intensity fluctuations were found to be 8.50% and 8.63% for the measurements with the CCD camera and the power meter respectively. These fluctuations (noise) would be detrimental in the later measurements and thus, it was necessary to use a normalization technique for suppressing the noise. In this technique, the intensity of the reflected beam measured by the power meter was utilized as the reference signal, while the transmitted

part of the beam was used for the actual experiments. The normalization was then achieved by taking the ratio of the intensity through the optical materials to the intensity of the reference signal as shown in equation 3.2.

$$\text{Normalization} = \frac{\text{Intensity (object beam)}}{\text{Intensity (reference beam)}} \qquad 3.2$$

As a demonstration, normalization to the reference signal (ratio of both intensities) of the already obtained data (appended in appendix 1) was performed and plotted in the graph shown in figure 3.2. The ratio of the two intensities as depicted by the blue curve shows a cancelling out. Thus, normalization process was successful and found to have suppressed the fluctuations to as low as 0.20%.

The graph in figure 3.2 enables a direct comparison for both of the beams as well as the ratio of their intensities. For that, the normalization was with respect to their respective maximum values.

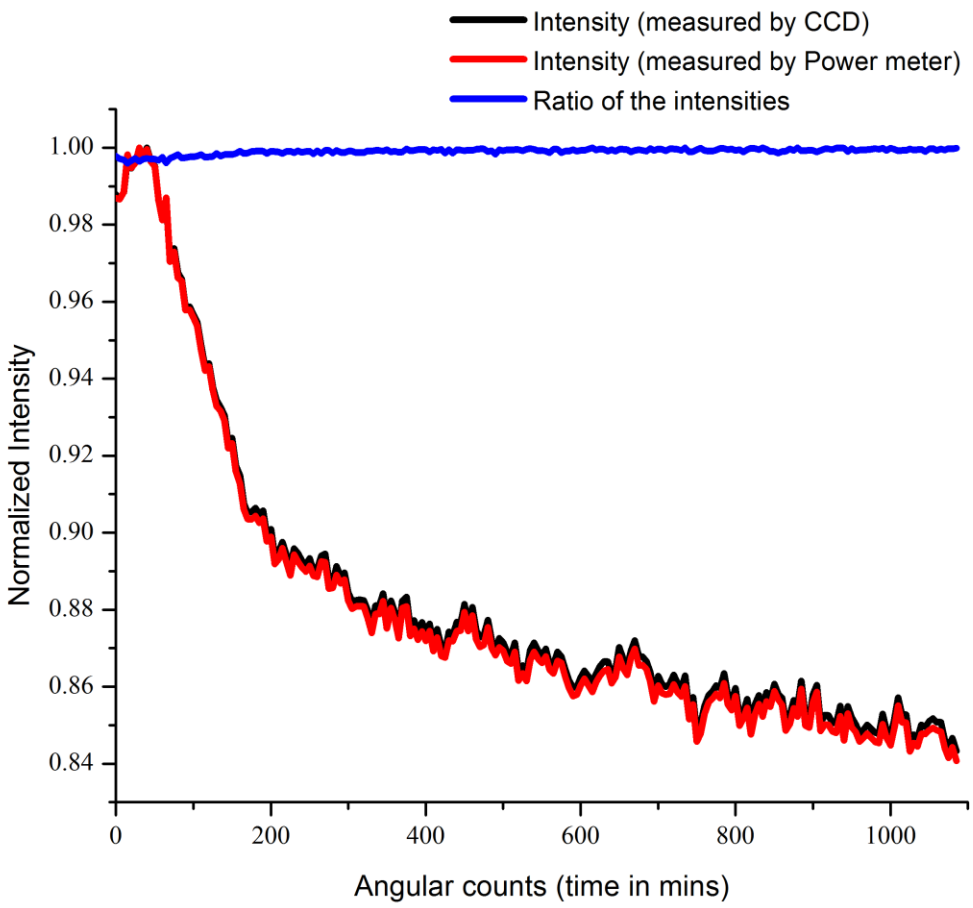

Figure 3.2: Graphs of the Normalized intensity against the angular counts of the beam measured by the power meter and the CCD camera. Both curves are normalized to their respective maximum value. Strong intensity fluctuations are evident for the reflected and transmitted beam. In contrast, the ratio between both intensities stays nearly constant.

3.2.2 Spatial filtering and beam magnification

Passing a laser beam through optical elements often introduces spatial intensity fluctuations to the initial beam profile because of dust, or imperfections of the optical elements. To provide a noise free beam, the laser beam was coupled into a Polarization maintaining fiber (PMF). The filtered beam behind the PMF emerged as a diverging beam and thus collimation of the beam was necessary. This was achieved by using a Microscope objective (MO) placed behind the PMF. Collimation ensures a low beam divergence.

The collimated beam was magnified as described in Section 2.3. This was to ensure that the beam covered a bigger portion of the cellophane sheet and to minimize the effect of a non-perfect central area of the polarization mask fabricated. A pinhole of diameter d = 20 µm was introduced in the focus between the two lenses to spatially filter the beam. The choice of the pinhole size is usually vital since a small pinhole would decrease the intensity of the beam which would reduce the measurement precision. On the other hand, the use of a large pinhole allows some noise (higher order modes) to be transmitted. Therefore, determining the optical pinhole size is very important. The appropriate pinhole size is determined using the simplified expression shown in equation 3.3.

$$\mathrm{D} = \frac{\lambda . f}{r}. \qquad 3.3$$

Where D is the pinhole diameter, λ is the wavelength, f is focal length of the lenses and r is the input beam's radius. For this research; $\lambda = 632.8\,nm$, $f = 80\,mm$, and $r = 3.75\,mm$. The pinhole was chosen so that it is approximately 30% larger than the value of the diameter calculated using equation 3.3 (Rosenzweig, 2003). Therefore, from the calculations the pinhole would ideally be 17.6 µm. However, a pinhole of 20 µm was used for the spatial filtering.

Since beam magnification is given by the ratio of the focal length of the output side to the focal length of the input side (as shown in equation 3.4), a doublet lens with a focal length of 160 mm was chosen and placed behind the spatial filter so that the collimated beam's diameter is magnified.

$$\text{Magnification} = \frac{f_2}{f_1} = \frac{160\,\text{mm}}{80\,\text{mm}} = 2. \qquad 3.4$$

Therefore, a magnification of the beam by a factor of 2 was achieved.

3.3 Analysis of the birefringence properties of the cellophane sheet

3.3.1 The cross-polarization test

Using the polariscope test described in section 2.4.1, images of the beam captured by the CCD camera were evaluated using both MATLAB and Origin pro softwares. By this, the intensity of each image of the beam depending on the rotation of the cellophane sheet(s) or the commercial HWP was determined. With aid of Origin pro software, graphs of normalized intensity versus the rotated angle were plotted and are presented in figures 3.3 to 3.5. Various cellophane sheets from different manufacturers were tested; some of them did not display the birefringence characteristics. However, the sheets that passed this test were evaluated and their corresponding graphs are presented in figure 3.3.

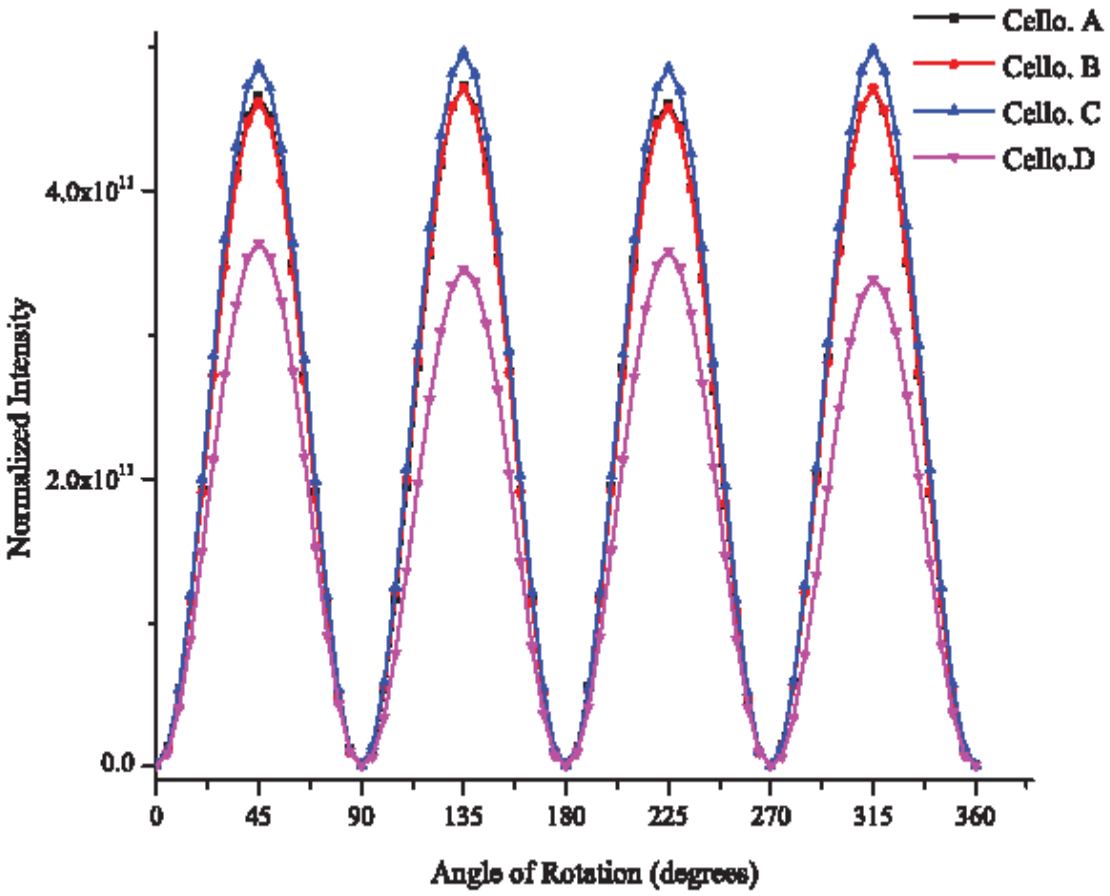

Figure 3.3: A graph of normalized intensity against the angle of rotation for the test sheets that displayed variation in the transmitted light upon rotation. A, B, C, and D represent cellophane sheets from different manufacturers. The intensity is normalized to the respective reference intensity.

The graph in figure 3.3 shows that the behavior of the cellophane sheet is dependent on the manufacturer. Cellophane A and B were chosen and happen to be from the same manufacturer and evidently displayed the same characteristic.

When the axes of the linear polarizers were set perpendicular to each other, no light was transmitted through the second polarizer (crossed polarization). Introducing the

cellophane between the polarizers and rotating it about the beam axis, it is observed that, depending on the angular orientation of the cellophane, light was passing through the second polarizer. However, there were two orientations of the cellophane sheet with an angular difference of 90 degrees which permitted no light to pass through the second polarizer. When the cellophane was turned halfway between these two orientations, the light transmitted through the second polarizer is the brightest as seen from the maximum intensities in figure 3.3.

Table 3.1 presents the maximum and minimum intensity values which have been extracted from the graph shown in figure 3.3. Using these values, modulation, which is a useful parameter in evaluating the performance of a system, was calculated for each of the cellophane samples tested. Modulation, also known as contrast and is defined by equation 3.5 (Hecht, 2002).

$$Modulation, M = \frac{I_{\max} - I_{\min}}{I_{\max} + I_{\min}}, \text{with } .0 \le M \le 1 \qquad 3.5$$

With this parameter, the polarization state of the measured beam through an optical element can be determined. Where, if M>0.9, the beam is classified as totally polarized and its degree of polarization considered to be equal to M (Mejias *et al.*, 2002). The average values obtained for the modulation was found to be; 0.9961, 0.9969, 0.9968, and 0.9952 for the beam through cellophanes' A, B, C and D respectively. Ideally, the modulation/contrast has a maximum value of 1. However, the value obtained in all the cellophane sheets tested is reduced as a result of diffraction and aberrations due to the surface.

Table 3.1: The maximum and minimum intensity values of the laser beam through the cellophane samples tested. Included also are the calculated modulation for all samples. The same laser power was used and the experiments performed with the same conditions.

Max. Normalized Intensity				**Min. Normalized Intensity**				**Modulation/Contrast**			
Cello A	**Cello B**	**Cello C**	**Cello D**	**Cello A**	**Cello B**	**Cello C**	**Cello D**	**Cello A**	**Cello B**	**Cello. C**	**Cello. D**
4.66 E+11	4.62 E+11	4.87 E+11	3.64 E+11	9.62 E+08	7.27 E+08	8.06 E+08	8.43 E+08	**0.9959**	**0.9969**	**0.9967**	**0.9954**
4.72 E+11	4.72 E+11	4.96 E+11	3.46 E+11	8.55 E+08	7.28 E+08	8.28 E+08	8.58 E+08	**0.9964**	**0.9969**	**0.9967**	**0.9951**
4.61 E+11	4.58 E+11	4.86 E+11	3.58 E+11	9.22 E+08	6.97 E+08	7.61 E+08	8.59 E+08	**0.9960**	**0.9970**	**0.9969**	**0.9952**
4.72 E+11	4.72 E+11	4.99 E+11	3.39 E+11	8.86 E+08	7.28 E+08	8.08 E+08	8.54 E+08	**0.9962**	**0.9969**	**0.9968**	**0.9950**

Even though cellophane A and B are from the same manufacturer and portray similar trend in the rotation of the incident light as shown in figure 3.3, their modulation values are different. This can be attributed to their respective coefficient of absorption, since in an anisotropic substance absorption can vary with the direction.

For further analysis and discussion, cellophane C was selected because it displays the largest variation in the transmitted light with rotation and has a high contrast. Along the 0°-180° axis and 90°-270° axis, the polarization seems to be unchanged, and the cross polarization configuration is preserved (shown in figure 3.3). Therefore, these two

orientations mark the orientation of the fast and/or slow axis of the apparently birefringent cellophane. This is because zero transmission occurs whenever the incident light polarization coincides with either the fast or slow axis. However, this test alone cannot be used to determine which axis is the fast and/or slow axis. To make this determination, the same experiment was performed using a commercial HWP whose fast and slow axes are well defined. Figure 3.3 enables a direct comparison of the commercial HWP with the cellophane sheet that displayed the largest variation in the transmitted light with rotation (well-behaved), cellophane C. The determination of the cellophane's axes (both the slow and the fast axis) was fundamental for this research. This would ensure proper positioning of the cellophane during the fabrication of the polarization mask. Consequently, the direction of polarization of the beam through the mask would be rotated as desired.

When both are oriented along the 0°- 180° axis and the 90°-270° axis, no transmission is observed whereas at an orientation halfway i.e., the 45^0-135^0 axis and the 225^0-315^0 axis , the transmission through the second polarizer is maximum (as depicted in figure 3.4). However, the commercial HWP recorded higher intensity values in comparison to the cellophane sheet even though the experiments were done practically with the same conditions. This behavior can be attributed to the presence of antireflection coatings on the commercial HWP (as illustrated in the specifications by Thorlabs Inc. and appended in appendix 5) which the cellophane sheet lacks. The antireflection coatings increase transmission by reducing surface reflectance loss. On the contrary, the cellophane sheet reflects some of its power and hence the transmitted power is reduced. Nevertheless, this formed the first proof that the cellophane sheet behaves similar to a commercial HWP.

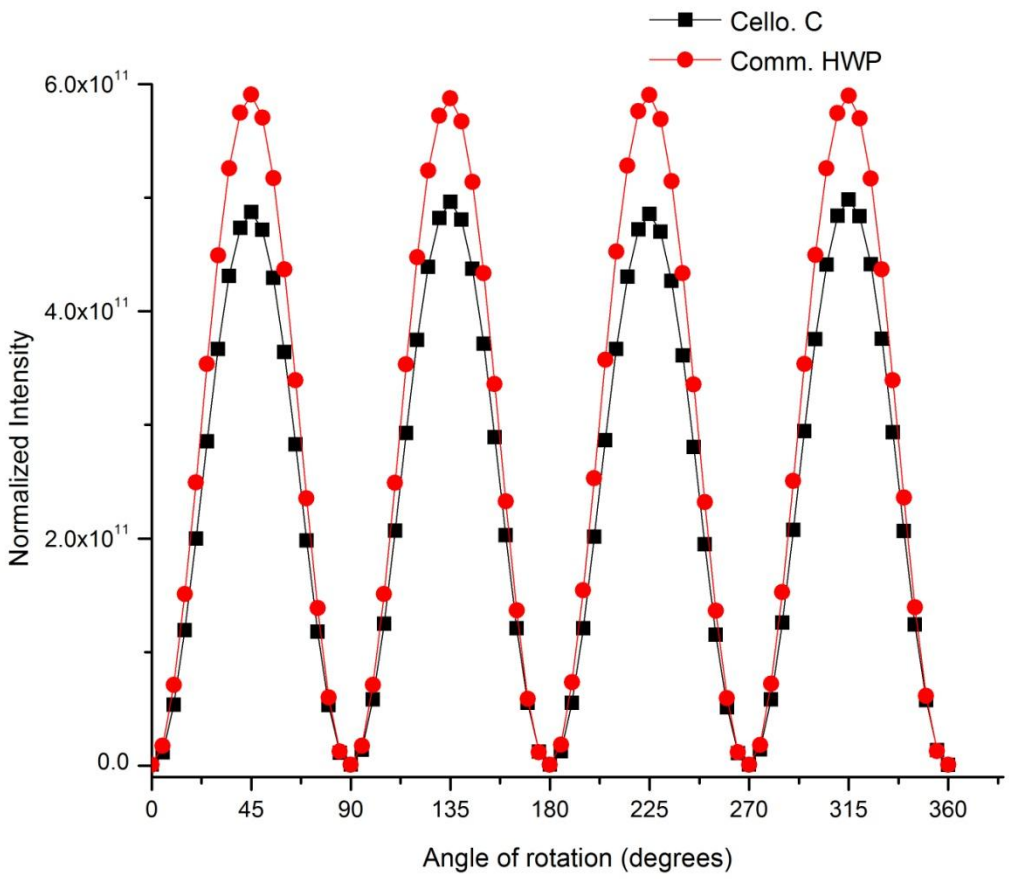

Figure 3.4: A graph of normalized intensity against the angle of rotation comparing the cellophane sheet with a commercial HWP. It can be seen that the cellophane sheet behaves almost like a purpose built HWP.

Using figure 3.4, the maximum and minimum intensity values for both cellophane and the commercial HWP are extracted and presented in table 3.2. Their modulation/contrast is evaluated using equation 3.5.

Table 3.2: The maximum and minimum intensity values of the laser beam through the cellophane sheet and the commercial HWP. Included also are the calculated modulation for both samples. The same laser power was used and the experiments performed with the same conditions.

Max. Normalized Intensity		Min. Normalized Intensity		Modulation/Contrast	
Cello.	**HWP**	**Cello.**	**HWP**	**Cello.**	**HWP**
4.87E+11	5.91E+11	8.06E+08	7.94E+08	0.9967	0.9973
4.96E+11	5.88E+11	8.28E+08	7.36E+08	0.9967	0.9975
4.86E+11	5.91E+11	7.61E+08	7.98E+08	0.9969	0.9973
4.99E+11	5.90E+11	8.08E+08	7.58E+08	0.9968	0.9974

The average values obtained for the modulation/contrast values are; 0.9968 and 0.9974 for the cellophane and commercial HWP respectively. These values are comparable and differ in the third significant digit, a good indication of the viability of an ordinary cellophane sheet to be used as a HWP.

3.3.2 Surface analysis

Images of the beam captured using the CCD camera when it was projected into the cellophane sheet and the commercial HWP are presented in figure 3.5 (a) and (b) respectively. The beam through the cellophane, figure 3.5(a) appears noisy and speckled in comparison to the one through the HWP (figure 3.5 (b)). This phenomenon occurs due to constructive and destructive interference from the small scattering centers within the area (cellophane surface) where the laser beam is incident (Dainty, 1975; Svelto, 2010). This is an indication that the surface of cellophane is extremely rough on the scale of an optical wavelength.

Speckle noise often constitutes an undesirable feature of coherent light (Svelto, 2010). For instance, the spatial resolution of the image of an object made through illumination with laser light is in fact often limited by speckle noise. In order to reduce this effect, the cellophane was sand-witched between two glass plates. The image captured is shown in figure 3.5 (c). A comparison with figure 3.5 (a), shows improvement in the quality of the beam and the speckle pattern is not visible in the image.

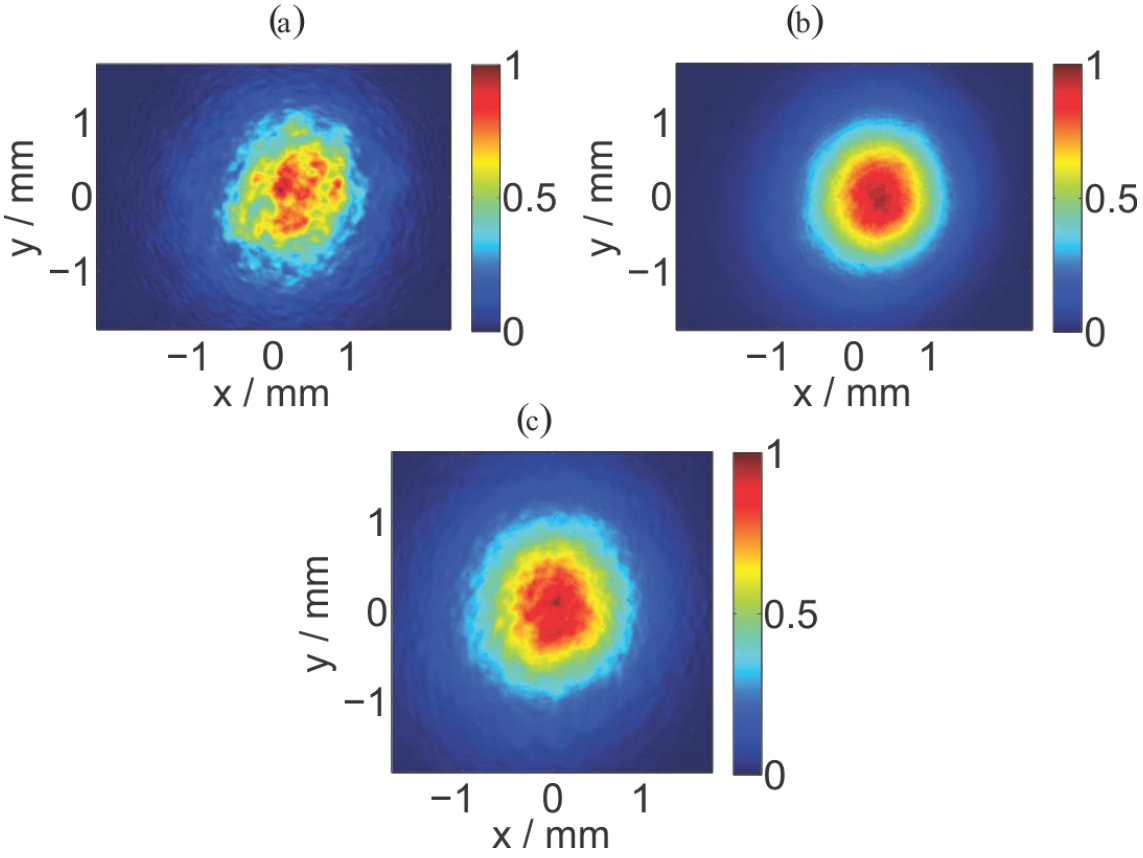

Figure 3.5: Images of the beams emerging through; (a) Cellophane sheet, (b) commercial HWP, and (c) cellophane in-between two glass plates. The beam going through the cellophane appears like the surface of an orange peel, while through the HWP and the cellophane-glass sandwich, the beam appears smooth and clean.

3.3.3 The Stokes parameters measurement for the cellophane sheet

Several methods to determine Stokes polarization parameters have been reported as discussed in section 1.4. For this research, the rotating quarter-waveplate (QWP) technique shown in figure 2.4 was used. This is because it is accurate and can be readily implemented. Besides, it avoids the limitations of the other methods in that more data points can be measured and that it allows a curve fitting algorithm to be used to determine the Stokes parameters (Schaefer *et al.,* 2007). The measurements presented in

this thesis were completely automated by use of Visual Basic software. Here, the rotatable QWP was controlled by a stepping motor interfaced to the computer so that a set of N (16) data points corresponding to the angular positions were obtained. The analysis of the data was done using MATLAB code shown in appendix 3. Section 1.4 describes the Stokes polarization parameters in detail.

The Stokes parameters extracted from the representative data scans for the light through the cellophane were;

$$\text{Cellophane} = \begin{pmatrix} S_0 = 1.0000 \\ S_1 = -0.9940 \\ S_2 = -0.0163 \\ S_3 = -0.1083 \end{pmatrix};$$ In comparison to the theoretical values for linearly polarized light which are; $= \begin{pmatrix} S_0 = 1.0000 \\ S_1 = -1.0000 \\ S_2 = 0.0000 \\ S_3 = 0.0000 \end{pmatrix}$

The beam through the cellophane possessed strong circular components (S_3 = 0.1083). This could be attributed to the poor surface structure (shown in section 3.2.2) as well as errors in alignment of the cellophane sheet. However, these results for the cellophane sheet compares very well with the expected theoretical value.

3.4 The fabricated polarization mask

For each polarization mask, four segments each with different orientation of the fast axis were joined together using immersion oil and fixed between two glass plates (shown in figure 2.5). This approach served a dual purpose. Because of adhesion forces, the four cellophane segments were fixed between the two glass plates (no additional glue is needed). Furthermore, wave front aberrations and speckles caused by the surface roughness of the Cellophane are reduced.

Figure 3.6 gives an illustration of the basic principle of the underlying polarization conversion. When a linearly polarized Gaussian beam is passed through the polarization mask, the polarization direction of the transmitted field is either unaltered or rotated by twice the angle of incidence. As such, either a pseudo-radially or pseudo-azimuthally polarized beam is obtained. The polarization state of the generated beam can be switched from radial to azimuthal, by simply rotating the polarization of the linearly polarized incoming beam from vertical to horizontal (as depicted in figure 3.6).

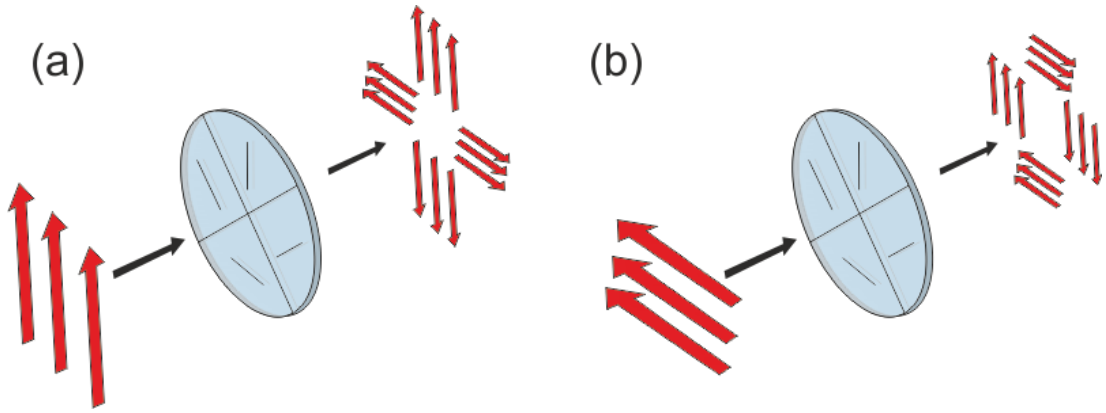

Figure 3.6: Working principle of a segmented wave plate-based polarization converter. Generation of a (a) (pseudo-) radially or (b) (pseudo-) azimuthally polarized light beam for a vertically or horizontally linearly polarized input beam respectively. (Quabis *et al.*, 2005)

3.5 Generated doughnut beams

The fabricated polarization mask described in section 2.5 was incorporated in the setup shown in figure 2.7 to convert a linearly polarized Gaussian beam into either radially or azimuthally polarized beam. When linearly polarized Gaussian beam was passed through the polarization mask, each segment with fast axis oriented differently, rotated locally the polarization of the incident linearly polarized beam so that a pseudo-doughnut beam was obtained (as explained in section 3.4). The pseudo-doughnut beam

is usually a mixture of pure radially or azimuthally polarized beams and some higher order modes (Maekawa & Uesaka, 2008; Yuzhao, 2009).

Figure 3.7 (a) shows the intensity distribution S_0 of the generated beam emerging from the polarization mask measured directly behind the mask before the spatial filtering. The four segments are clearly visible in the diffraction pattern.

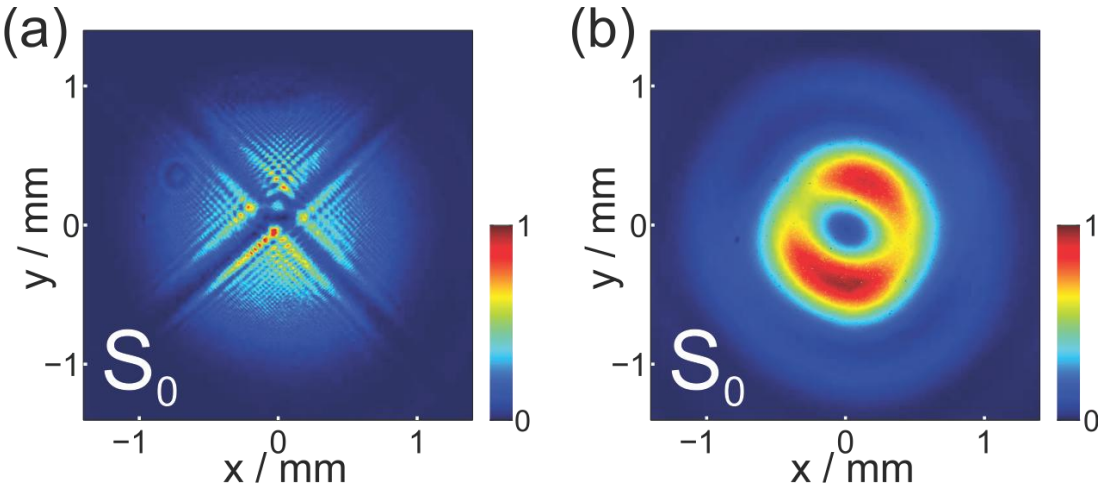

Figure 3.7: (a) Intensity profile of an incoming linearly polarized light beam immediately after passing through the polarization mask. (b) The high quality vector beam obtained after spatial filtering.

The pseudo-radially polarized beam obtained immediately after the polarization mask has a poor mode quality (as shown in figure 3.7 (a)). This is due to the fact that the mask with the cellophane segments introduces abrupt changes at the edges and the impinging light beam is scattered and diffracted at these edges. In addition, the limited number of segments as well as the ordinary overlap between the intensity distributions of the incoming and the desired beam results in the generation of higher order modes (Quabis *et al.*, 2005). When introducing the pinhole filtering (as described in section 2.6, figure 2.7), the quality of the generated mode can be increased significantly as shown in figure 3.7 (b). Alternatively, the mode purity can also be improved by letting the beam emerging from the mask propagate for several meters. Due to the fact, that higher order

modes diffract more rapidly, the central part of the beam close to the optical axis purifies.

The pinhole size used for the filtering had a larger diameter (d = 30 μm) compared to the pinhole used in filtering the fundamental Gaussian beam, TEM_{00} mode. This was done in order to increase the transmission of the radially or azimuthally polarized modes, consisting of the higher order TEM_{01} mode, which is the first higher order mode.

The high quality beam obtained after spatial filtering (shown in figure 3.7 (b)), was analyzed using Origin Pro software. A cross section of the beam intensity profile along the radial direction obtained is presented in figure 3.8.

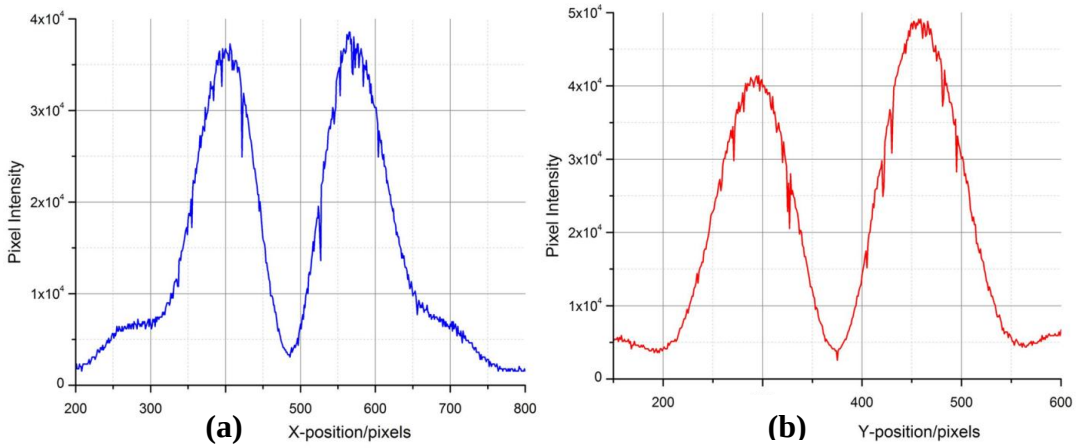

Figure 3.8: Intensity cross sections of the doughnut beam (a) in the horizontal direction, and (b) the vertical direction.

The experimentally determined mode shape along the y-direction shows uneven edges in intensity distribution. This asymmetry can be attributed to the non-perfectness' in joining of the segments making up the polarization mask as well as errors in alignment of the cellophane. Nevertheless, both the intensity profiles shown in figure 3.8 and the intensity cross sections of figure 3.9 give an indication that the beam generated from the fabricated polarization mask was indeed a doughnut beam.

3.6 Analyzing the polarization state of the generated doughnut beam

3.6.1 Using a rotating linear polarizer

The polarization state of the generated beam (shown in figure 3.7 (b)) was analyzed by capturing image of the beam profile after passing through a rotatable linear polarizer using a CCD camera. A two-lobe pattern with a dark bar in between was obtained as shown in figure 3.9. These patterns were seen to rotate in the same direction with respect to the direction of the polarizer. This was the first indication that the generated beams have polarization order number +1. For beams with polarization order number -1, the lobes would have rotated in the opposite direction with the rotation of the linear polarizer (Kozawa & Sato, 2005). With the linear polarizer in the beam path, only the projections of the mode that are aligned with the polarizer axis are transmitted leading to the two lobe patterns.

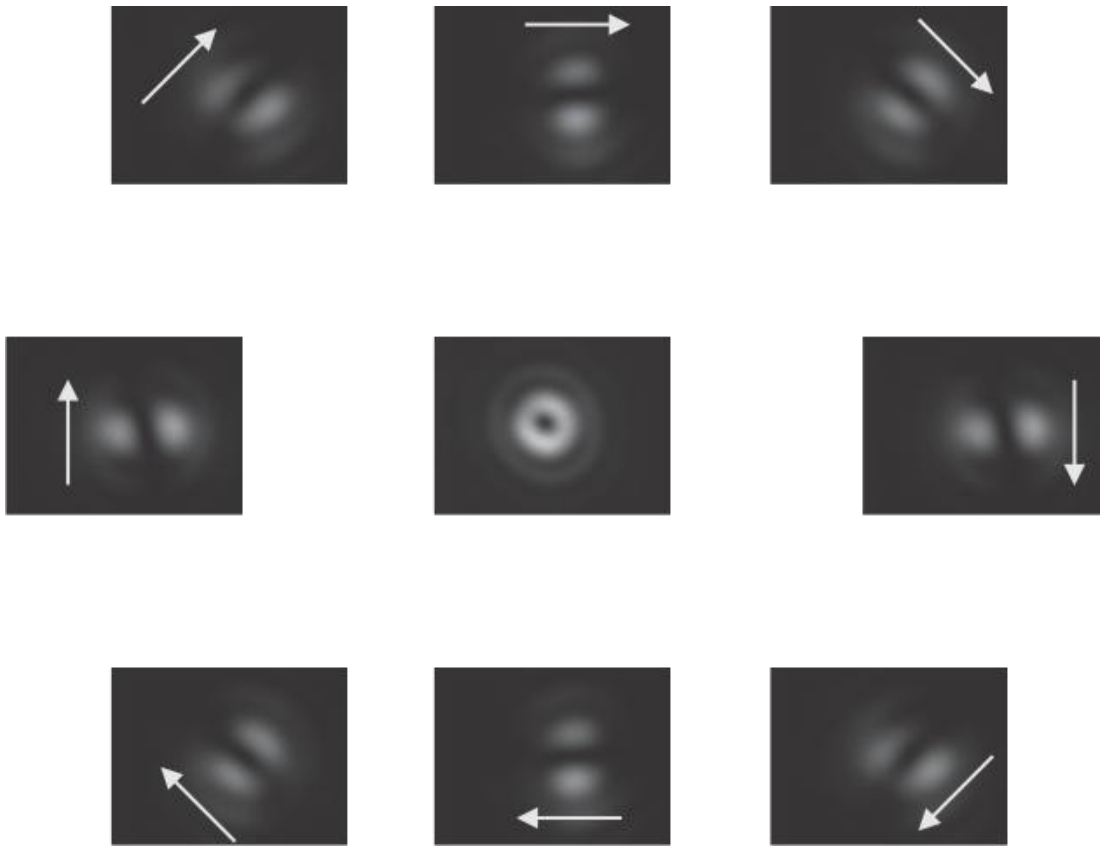

Figure 3.9: Experimental image of the generated azimuthally polarized beam that emerge from the fabricated polarization mask after passing through the rotatable linear polarizer. The central image of the beam was obtained without the polarizer. The transmission axis of the polarizer is indicated by the arrows in the respective images.

Figure 3.9 shows the image patterns of the doughnut beam after passing through the rotating linear polarizer whose transmission axis was oriented as indicated by the arrows. The 2-lobe image patterns with a dark bar in between are along a line perpendicular to the polarization direction, as expected for an azimuthally polarized beam.

When a radially polarized beam was passed through the rotatable linear polarizer, image patterns (as presented in figure 3.10) were obtained. The two lobes image patterns with a

dark bar in between are aligned along the polarization direction of the polarizer in each image, as expected for a radially polarized beam.

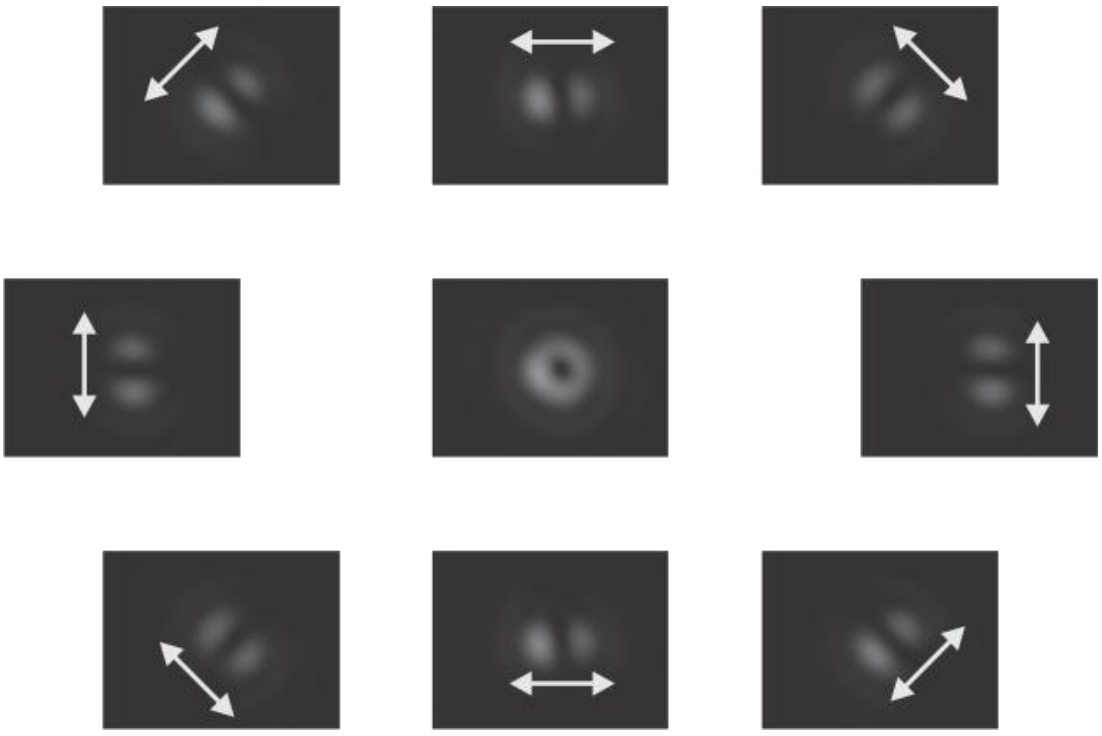

Figure 3.10: Experimental image patterns of the generated radially polarized beam that emerge from the fabricated polarization mask after passing through the rotatable linear polarizer. The central image of the beam was obtained without the polarizer. The transmission axis of the polarizer is indicated by the arrows in the respective images.

Ideally, after passing a doughnut beam through a rotating linear polarizer, the emerging image patterns must have two lobes with a dark bar in between. The two lobes are usually perpendicular to the polarization direction of the linear polarizer for the case of azimuthally polarized beams and parallel for radially polarized (Oron *et al.,* 2000; Passily *et al.,* 2005).

3.6.2 Measurement of Stokes polarization parameters of the generated doughnut beams

To quantify the polarization purity of the generated doughnut beam, the Stokes parameters S_0, S_1, S_2 and S_3 spatially resolved were measured using the setup shown in figure 2.7. S_0 represents the total intensity, while S_1 and S_2 describe the linear polarization in the horizontal-vertical basis and in the diagonal-anti-diagonal basis, respectively. S_3 quantifies the amount of circular polarization. Section 1.4 described these parameters in detail. The values obtained for the generated radial beam were; S_0 = 1.0000, S_1 = 0.0884, S_2 = 0.1352, and S_3 = 0.0472, in comparison to the values S_0 = 1.0000, S_1 = 0.0000, S_2 = 0.0000, and S_3 = 0.0000, associated with a pure radially polarized beam. The deviation in the values (error) is associated mainly with the non-perfect nature of the cellophane as a HWP (as depicted in section 3.3), errors due to alignment of the cellophane and small imperfections of the polarization mask. However, these values are a good indicator of a doughnut mode.

Figure 3.11 shows the spatial distribution of the experimentally obtained normalized Stokes parameters S_0, S_1, S_2 and S_3 of the filtered radially polarized beam, with the insets illustrating the theoretically expected distributions.

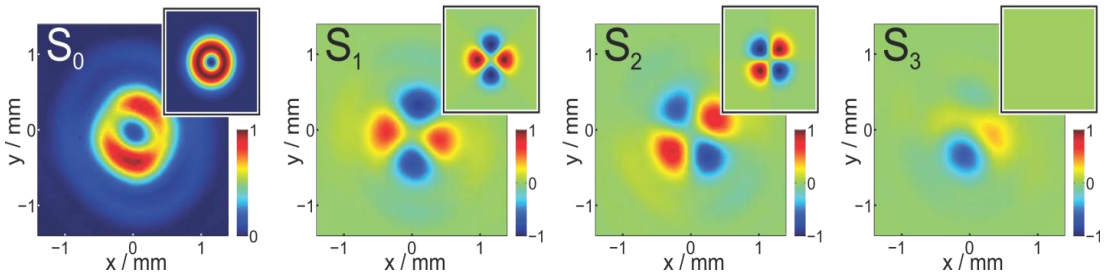

Figure 3.11: Experimentally measured and calculated (insets) distributions of the spatially resolved Stokes parameters S_0, S_1, S_2 and S_3 of a radially polarized beam. All Stokes parameters are normalized to the maximum value of S_0.

Considering the intensity profile of the beam, the typical ring-like distribution of the S_0 parameter can be seen. The small deviations from the theoretical intensity distribution are caused by residual higher order modes, which are not filtered out by the pinhole. Additionally, lower intensity circular polarization components are evident, although S_3 should be exactly zero everywhere in the plane of observation. This deviation is likewise attributed to the small imperfections of the mask. The linear polarization distributions S_1 and S_2, however, show a very good overlap with the respective theoretical prediction, clearly indicating the generation of a good quality radially polarized beam.

CHAPTER FOUR

4.0 SUMMARY, CONCLUSION AND RECOMMENDATIONS

4.1 Summary

By considering that cellophane is not purposely built to perform as a half waveplate, it behaves exceptionally well in comparison to a commercial HWP, thus providing an alternative to the commercial HWP, especially in applications that are not critical to surface aberrations. It may have an advantage over a commercial HWP when it comes to broad band operation. This is because commercial HWPs are designed to operate at a particular center wavelength and if one deviates from this value, the HWP no longer exhibits its properties. However, on transmitting a beam through a cellophane sheet and a HWP, a lower maximum power was exhibited than with a commercial HWP.

Having identified the cellophane sheet(s) with the desired birefringence properties, a polarization mask was fabricated. Such a polarization mask consisted of four segments each with different orientation of the fast axis. The segments were sandwiched between two microscope cover slips (glass) for support. Immersion oil was inserted in between so as to match the refractive index of the glasses as well as gluing the segments together. The performance of the mask as a mode and polarization converter was tested experimentally.

After wards, a linear setup was designed for the conversion of a linearly polarized Gaussian into a radially or azimuthally polarized beam. A HWP was placed in the beam path before the polarization mask so as to rotate the polarization of the input linearly polarized beam into either vertical or horizontal such that either radial or azimuthal beams were generated. The spatially filtered, expanded and collimated laser was guided through the polarization mask, which converted a vertically polarized Gaussian beam to a pseudo-radially polarized beam and a horizontally polarized Gaussian beam to a pseudo-azimuthally polarized beam. It was observed that, the generated beam obtained immediately after the polarization mask had a poor mode quality. This was attributed to

the limited number of segments and that the cellophane segments introduced abrupt changes in the transverse beam properties thus the impinging light beam was scattered and diffracted at these edges. In order to achieve high mode purity of the generated beams, a spatial filter was used to filter out higher order modes while preserving the radial or azimuthal polarization components. The spatial filter comprised of two lenses and a pinhole of diameter 30 μm.

The polarization state of the generated beam was analyzed by passing through a rotatable linear polarizer. The image patterns/lobes emerging from the polarizer were captured using a CCD camera interfaced to a computer. A two-lobe pattern with a dark bar in between was obtained. These patterns were seen to rotate in the same direction with respect to the direction of the polarizer as expected for beams with polarization order number +1. The 2-lobe image patterns with a dark bar in between were along a line perpendicular to the polarization direction, as expected for an azimuthally polarized beam. When radially polarized beam was passed through the rotatable linear polarizer, the two lobes image patterns with a dark bar in between were everywhere aligned along the polarization direction of the polarizer.

The polarization purity was quantified by taking the Stokes measurements. The values obtained for the generated radial beam were; $S_0 = 1.0000$, $S_1 = 0.0884$, $S_2 = 0.1352$, and $S_3 = 0.0472$, showing a good agreement with the values $S_0 = 1.0000$, $S_1 = 0.0000$, $S_2 = 0.0000$, and $S_3 = 0.0000$, associated with a pure radially polarized beam. Additionally, the spatial distribution of the experimentally normalized Stokes parameters S_0, S_1, S_2 and S_3 of the radially polarized beam were compared with the theoretically expected distributions. Small deviations from the theoretical intensity distributions for the S_3 components were seen. However, the S_1 and S_2 components had a very good overlap with the respective theoretical prediction, clearly indicating the generation of a good quality radially polarized beam.

4.2 Conclusion

The research was successful since beams with polarization order number +1 were generated from a linearly polarized beam using the cellophane-made polarization mask. To the best of our knowledge, this is the first polarization converter to be fabricated from a cellophane sheet. The polarization masks are easy to fabricate and the use of cellophane sheets makes this technique easily achievable and cost effective. In order to put the cost effectiveness into perspective, a short consideration of the actual costs of the mask seems appropriate. Two microscope cover slips (0.3 US Dollar), two droplets of immersion oil (0.1 US Dollar), and roughly $10mm^2$ of Cellophane (1 m^2 costs approximately 0.3 US Dollar) were used. Even though large areas of different cellophane sheets were used in the search for the one with the desired birefringence properties, the actual cost for fabricating a single polarization mask is below 1 US Dollar.

The success of this project is a major step forward especially for upcoming institutions in the field of Optics and Lasers physics. This approach can be readily implemented and has the advantage of being cheap, reliable and allowing existing lasers to be used. Additionally, this approach provides a simple and robust method to generate both TEM_{10} and TEM_{01} modes.

4.3 Recommendations

The quality of the doughnut beam generated using the SVR technique is dependent on the number of segments used (Quabis *et al.*, 2005). Therefore, as future work in this approach the number of segments of the polarization mask can be increased to enhance the mode overlap of the incoming and the desired beam. Additionally, the mode purity can also be improved by letting the beam emerging from the mask propagate for several meters instead of using the pinhole spatial filter. Due to the fact, that higher order modes diffract more rapidly, the central part of the beam close to the optical axis purifies.

Further work can also be done especially applying anti-reflection coatings on the cellophane sheet. This will reduce the diffuse reflections on the sheet and make it a

better HWP which could be used in fabrication of better polarization masks. This will in turn increase the quality and efficiency of the doughnut beam generated.

REFERENCES

Ahmed M., Andreas V., Vogel M., Austerschulte A., Schulz J., Metsch V., Moser T., and Graf T. (2009). Radially polarized high-power lasers**.** *Proceedings of SPIE,* **7131** (111), 1-10.

Berry H., Gabrielse G., and Livingston A. (1977). Measurement of the Stokes parameters of light. *Applied Optics,* **16** (12), 3200-3205.

Biss D., and Brown T. (2001). Cylindrical vector beam focusing through a dielectric interface. *Optics Express,* **9**, 77.

Born M., and Wolf E. (1999). *Principles of Optics,* (7th ed.). Cambridge: Cambridge University press.

Collet E. (1968). The description of polarization in classical physics. *American Journal of Physics,* **36,** 713-725.

Collet E. (1992). *Polarized Light; Fundamentals and Applications*. New York: Marcel Dekker.

Dainty J.C. (1975). *Laser Speckle and related Phenomena.* Berlin: Springer-verlag.

Dorn R., Quabis S., and Leuchs G. (2003). Sharper focus for radially polarized light beam. *Physics Review Letters,* **91** (233901), 1-4.

Edwards S., and Langley A. (1981). On Producing Colors Using Birefringence Property of Transparent, Colorless Stretched Cellophane. *Leonardo,* **14** (3), 187-190.

Ellenbogen T., Wang D., and Kenneth B. (2012). Generation of quasi-coherent cylindrical vector beams by leaky mirror less laser. *Optics Express,* **20** (27), 28862-28870.

Hao X., Kuang C., Wang T., and Liu X. (2010). Effects of polarization on the de-excitation dark focal spot in STED microscopy. *Journal of Optics,* **12,** 115707.

Hecht E. (2001). *Optics,* (4th ed.). London: Addison Wesley Reading.

Iizuka K. (2003). Cellophane as a half-wave plate and its use for converting a laptop computer screen into a 3D display. *Review of Scientific Instruments,* **74** (8), 3636-3639.

Iizuka K. (2012). Complementary cellophane optic gate and its use for a 3D ipad without glass. *Review of scientific Instruments,* **83** (043710), 1-3.

Kindler J., Banzer P., Quabis S., Peschel U., and Leuchs G. (2007). Waveguide properties of single subwavelength holes demonstrated with radially and azimuthally polarized light. *Applied Physics B,* **89,** 517-520.

Kozawa Y., and Sato S. (2010). Optical trapping of micrometer-sized dielectric particles by cylindrical vector beams. *Journal of Optics,* **18** (10), 10828-10833.

Kozawa Y., and Sato S., (2005). Generation of a radially polarized laser beam by use of a conical Brewster prism. *Optics Letters,* **30**, (22), 3063-3065.

Kozawa Y., Yonezawa K., and Sato S. (2007). Radially polarized laser beam from a Nd:YAG laser cavity with a c-cut YVO4 crystal. *Applied Physics B,* **88**, 43–46.

Krishnan V., and Tan B. (2012). Generation of Radially Polarized Beam for Laser Micromachining. *Journal of Laser Micro/Nanoengineering,* **7** (3), 274-278.

Machavariani G., Lumer Y., Moshe I., Meir A., and Jackel S. (2007). Efficient extra cavity generation of radially and azimuthally polarized beams. *Optics Letters,* **32** (11), 1468-1470.

Maekawa A., and Uesaka M. (2008). Generation of Radial Polarized Laser Beam and its Applications for Accelerator. *Proceedings of FEL08,* **8** (082), 435-438.

Martinez-Herrero R., Mejias P.M., and Piquero G. (2009). *Characterization of Partially Polarized Light Fields.* Berlin: Springer-verlag.

Maurer C., Jesacher A., Fürhapter S., Bernet S., and Ritsch-Marte M. (2007). Tailoring of arbitrary optical vector beams. *New journal of Physics,* **9** (78).

Mejias P.M., Martinez-Herrero R., Piquero G., and Movilla J.M. (2002). Parametric characterization of the spatial structure of non-uniformly polarized laser beams, *Progress in Quantum Electronics*, (26), 65–130.

Miyaji G., Miyanaga N., Koji T., Sueda K., and Ken O. (2004). Intense longitudinal electric fields generated from transverse electromagnetic waves, *Applied Physics Letters,* **84** (19), 3855-3857.

Moser T., Balmer J., Delbeke D., Muys P., Verstuyft S., and Baets R. (2006). Intracavity generation of radially polarized CO2 laser beams based on a simple binary dielectric diffraction grating. *Applied Optics,* **45** (33), 8517- 8520.

Moshe I., Jackel S., Meir A., Lumer Y., and Leibush E. (2007). 2 kW, M^2<10 radially polarized beams from aberration-compensated rod-based Nd:YAG lasers. *Optics Letters,* **32** (1), 47-49.

Mushiake Y., Matsumura K., and Nakajima N. (1972). Generation of Radially Polarized Optical Beam Mode by Laser Oscillation. *Proceedings of the IEEE*, **60,** 1107.

Neil M.A.A., Massoumian F., Juskaitis R., and Wilson T. (2002). Method for the generation of arbitrary complex vector wave fronts. *Optics Letters*, **27,** 1929-31.

Nesterov A.V., and Niziev V.G. (2000). Laser beams with Axially Symmetric Polarization. *Journal of Physics D_Applied Physics*, **33,** 1817-1822.

Niziev V., and Nesterov V. (1999). Influence of beam polarization on laser cutting efficiency. *Journal of Physics D*, **32**, 1455-1461.

Niziev V., Chang R., and Nesterov A. (2006). Generation of in homogeneously polarized laser beams by use of a Sagnac interferometer. *Applied Optics,* **45** (33), 8393-97.

Oron R., Shmuel B., Davidson N., and Asher A. (2000). The formation of laser beams with pure azimuthal or radial polarization. *Applied Physics Letters,* **77** (21), 3322-3324.

Ortiz-Gutierrez M., Olivares-Peres A., and Sanchez V. (2001). Cellophane film as half wave retarder of wide spectrum. *Optical Materials,* **17,** 395-400.

Passilly N., Denis R., and Kamel A. (2005). Simple interferometric technique for generation of a radially polarized light beam. *Journal of the Optical Society of America A,* **22** (5), 984-991.

Pereira S., and Van de Nes A. (2004). Super resolution by means of polarization, phase and amplitude pupil masks. *Optics Communications,* **234,** 119-124.

Pohl D. (1972). Operation of a Ruby laser in the purely transverse electric mode TE01. *Applied Physics Letter,* **20**, 266–267.

Powell J., and Kaplan A. (2004). Laser Cutting: From first principles to the state of the art. *1st Pacific International Conference on Application of Lasers and Optics.* United Kingdom: Laser Expertise Ltd.

Quabis S., Dorn R., and Leuchs G. (2005). Generation of a radially polarized doughnut mode of high quality. *Applied Physics B,* **81,** 597-600.

Quabis S., Dorn R., Eberler M., Glöckl O., and Leuchs G. (2000). Focusing light to a tighter spot. *Optics communications,* **179,** 1-7.

Quabis S., Dorn R., Eberler M., Glöckl O., and Leuchs G. (2001). The focus of light – theoretical calculation and experimental tomographic reconstruction. *Applied Physics B,* **72,** 109-113.

Romea D., and Kimura D. (1990). Modeling of inverse Cerenkov laser acceleration with axicon laser-beam focusing. *Physical Review D,* 42 (5), 1807-18.

Rosenzweig J.B. (2003). *Fundamentals of Beam Physics*. New York: Oxford University Press.

Rurimo G.K. (2006). *Probing the focal region of highly focused laser beams using a quantum Well Heterostructure.* PhD Thesis, University of Erlangen-Nurnberg, Germany.

Rurimo G.K., Schardt M., Quabis S., Malzer S., Dotzler C.H., Winkler A., Leuchs G., Döhler G.H., Driscoll D., Hanson M., Gossard A.C., and Pereira S.F. (2006). Using a quantum well heterostructure to study the longitudinal and transverse electric field components of a strongly focused laser beam. *Journal of Applied Physics,* 100 (023112), 1-6.

Sancho-Parramon J., and Bosch S. (2012). Dark Modes and Fano Resonances in Plasmonic Clusters Excited by Cylindrical Vector Beams. *ACS Nano*, **6,** 8415-8423.

Schaefer B., Collet E., Smyth R., Barret D., and Fraher B. (2007). Measuring the Stokes polarization parameters. *American Journal of Physics,* **75** (2), 163-168

Scully M., and Zubairy M. (1991). Simple laser accelerator: Optics and particle dynamics. *Physical Review A,* **44** (4), 2656-2663.

Stalder M., and Schadt M. (1996). Linearly polarized light with axial symmetry generated by liquid-crystal polarization converters. *Optics Letters,* **21** (23), 1948-1950

Steen W.M., and Mazumder J. (2010). *Laser Material Processing*, (4th ed.). London: Springer-verlag.

Svelto O. (2010). *Principles of Lasers*, (5th ed.). London: Springer-verlag.

Tidwell S.C., Ford D.H., and Kimura W.D. (1990). Generating radially polarized beams interferometrically. *Applied Optics,* **29** (15), 2234-2239.

Volpe G., and Petrov D. (2004). Generation of cylindrical vector beams with few-mode fibers excited by Laguerre–Gaussian beams. *Optics Communications,* **237**, 89–95.

Xiangping L., Cao Y., and Gu M. (2011). Superresolution-focal-volume induced 3.0 Tbytes/disk capacity by focusing a radially polarized beam. *Optics Letters,* **36** (13), 2510-2512.

Youngworth K., and Brown T. (2000). Focusing of high numerical aperture cylindrical-vector beams. *Optics Express,* **7** (2), 80-87.

Yuzhao M. (2009). *Characterization of Higher Order Modes in Optical Fibers*. PhD Thesis, University of Erlangen-Nurnberg, Germany.

Zhan Q. (2004). Trapping metallic Rayleigh particles with radial Polarization. *Optics Express,* **12** (15), 3377-3382

Zhan Q., and Leger J. (2002). Microellipsometer with radial symmetry. *Applied Optics*, **41**, 4630–4637

Zhan Q. (2009). Cylindrical vector beams; from mathematical concepts to applications. *Advances in Optics and Photonics,* **1** (1), 1–57.

APPENDICES

Appendix 1: Table of the power analysis of the He-Ne laser used for the experiments. A power meter was used to measure the power of the reflected part of the beam while a CCD camera was used to capture the images of the transmitted part of the beam. The images were fed into Origin software which evaluated the intensity.

Angular counts	Intensity (CCD)	Intensity (PM)	Norm. intensity
0	3.61E+07	5.28E-07	6.831E+13
5	3.60E+07	5.28E-07	6.826E+13
10	3.61E+07	5.29E-07	6.824E+13
15	3.64E+07	5.34E-07	6.818E+13
20	3.63E+07	5.32E-07	6.823E+13
25	3.64E+07	5.33E-07	6.827E+13
30	3.65E+07	5.35E-07	6.822E+13
35	3.64E+07	5.33E-07	6.825E+13
40	3.65E+07	5.35E-07	6.827E+13
45	3.64E+07	5.33E-07	6.826E+13
50	3.63E+07	5.32E-07	6.826E+13
55	3.60E+07	5.28E-07	6.824E+13
60	3.58E+07	5.25E-07	6.829E+13
65	3.60E+07	5.28E-07	6.819E+13
70	3.54E+07	5.19E-07	6.827E+13
75	3.55E+07	5.20E-07	6.83E+13
80	3.53E+07	5.17E-07	6.833E+13
85	3.53E+07	5.16E-07	6.827E+13
90	3.50E+07	5.12E-07	6.828E+13
95	3.50E+07	5.12E-07	6.83E+13
100	3.49E+07	5.11E-07	6.829E+13
105	3.48E+07	5.10E-07	6.831E+13

Angular counts	Intensity (CCD)	Intensity (PM)	Norm. intensity
550	3.17E+07	4.63E-07	6.84E+13
555	3.18E+07	4.64E-07	6.84E+13
560	3.16E+07	4.62E-07	6.84E+13
565	3.16E+07	4.62E-07	6.84E+13
570	3.17E+07	4.64E-07	6.84E+13
575	3.17E+07	4.63E-07	6.84E+13
580	3.16E+07	4.61E-07	6.84E+13
585	3.15E+07	4.60E-07	6.84E+13
590	3.14E+07	4.59E-07	6.84E+13
595	3.14E+07	4.59E-07	6.84E+13
600	3.15E+07	4.60E-07	6.84E+13
605	3.15E+07	4.61E-07	6.84E+13
615	3.14E+07	4.59E-07	6.85E+13
620	3.15E+07	4.61E-07	6.84E+13
625	3.16E+07	4.62E-07	6.84E+13
630	3.16E+07	4.62E-07	6.84E+13
635	3.16E+07	4.62E-07	6.84E+13
640	3.15E+07	4.61E-07	6.84E+13
645	3.16E+07	4.61E-07	6.84E+13
650	3.18E+07	4.64E-07	6.84E+13
655	3.17E+07	4.63E-07	6.84E+13
660	3.16E+07	4.62E-07	6.84E+13

110	3.46E+07	5.07E-07	6.833E+13	665	3.17E+07	4.64E-07	6.84E+13
115	3.44E+07	5.04E-07	6.829E+13	670	3.18E+07	4.65E-07	6.84E+13
120	3.45E+07	5.05E-07	6.83E+13	675	3.17E+07	4.63E-07	6.84E+13
125	3.42E+07	5.01E-07	6.83E+13	680	3.17E+07	4.63E-07	6.84E+13
130	3.41E+07	4.99E-07	6.836E+13	685	3.16E+07	4.62E-07	6.84E+13
135	3.40E+07	4.98E-07	6.831E+13	690	3.15E+07	4.61E-07	6.84E+13
140	3.40E+07	4.97E-07	6.834E+13	695	3.13E+07	4.58E-07	6.84E+13
145	3.37E+07	4.93E-07	6.834E+13	700	3.15E+07	4.60E-07	6.84E+13
150	3.37E+07	4.94E-07	6.834E+13	705	3.14E+07	4.59E-07	6.84E+13
155	3.35E+07	4.90E-07	6.836E+13	710	3.14E+07	4.59E-07	6.84E+13
160	3.34E+07	4.88E-07	6.84E+13	715	3.14E+07	4.59E-07	6.84E+13
165	3.31E+07	4.85E-07	6.836E+13	720	3.15E+07	4.60E-07	6.84E+13
170	3.30E+07	4.83E-07	6.836E+13	725	3.14E+07	4.59E-07	6.84E+13
175	3.31E+07	4.83E-07	6.839E+13	730	3.14E+07	4.59E-07	6.84E+13
180	3.31E+07	4.84E-07	6.84E+13	735	3.15E+07	4.60E-07	6.85E+13
185	3.30E+07	4.83E-07	6.84E+13	740	3.11E+07	4.56E-07	6.84E+13
190	3.31E+07	4.83E-07	6.839E+13	745	3.13E+07	4.58E-07	6.84E+13
195	3.28E+07	4.80E-07	6.836E+13	750	3.10E+07	4.52E-07	6.84E+13
200	3.29E+07	4.81E-07	6.839E+13	755	3.10E+07	4.54E-07	6.85E+13
205	3.26E+07	4.77E-07	6.839E+13	760	3.12E+07	4.56E-07	6.84E+13
210	3.27E+07	4.78E-07	6.838E+13	765	3.13E+07	4.58E-07	6.84E+13
215	3.28E+07	4.79E-07	6.836E+13	770	3.13E+07	4.58E-07	6.84E+13
220	3.27E+07	4.77E-07	6.839E+13	775	3.14E+07	4.59E-07	6.84E+13
225	3.25E+07	4.75E-07	6.84E+13	780	3.14E+07	4.58E-07	6.84E+13
230	3.27E+07	4.78E-07	6.837E+13	785	3.15E+07	4.61E-07	6.84E+13
235	3.27E+07	4.77E-07	6.84E+13	790	3.13E+07	4.58E-07	6.84E+13
240	3.26E+07	4.77E-07	6.838E+13	795	3.13E+07	4.57E-07	6.84E+13
245	3.26E+07	4.76E-07	6.839E+13	800	3.14E+07	4.59E-07	6.84E+13
250	3.26E+07	4.77E-07	6.84E+13	805	3.11E+07	4.55E-07	6.84E+13
255	3.25E+07	4.75E-07	6.835E+13	810	3.12E+07	4.56E-07	6.84E+13
260	3.25E+07	4.75E-07	6.84E+13	815	3.13E+07	4.57E-07	6.84E+13
265	3.26E+07	4.77E-07	6.835E+13	820	3.10E+07	4.53E-07	6.84E+13

270	3.27E+07	4.77E-07	6.841E+13	825	3.12E+07	4.56E-07	6.84E+13
275	3.24E+07	4.74E-07	6.841E+13	830	3.13E+07	4.58E-07	6.84E+13
280	3.24E+07	4.74E-07	6.836E+13	835	3.12E+07	4.56E-07	6.85E+13
285	3.25E+07	4.76E-07	6.841E+13	840	3.13E+07	4.58E-07	6.84E+13
290	3.24E+07	4.74E-07	6.837E+13	845	3.13E+07	4.57E-07	6.84E+13
295	3.25E+07	4.75E-07	6.837E+13	850	3.14E+07	4.59E-07	6.84E+13
300	3.23E+07	4.72E-07	6.84E+13	855	3.13E+07	4.58E-07	6.84E+13
305	3.22E+07	4.71E-07	6.84E+13	860	3.13E+07	4.58E-07	6.84E+13
310	3.22E+07	4.71E-07	6.837E+13	865	3.10E+07	4.54E-07	6.84E+13
315	3.22E+07	4.71E-07	6.837E+13	870	3.11E+07	4.55E-07	6.84E+13
320	3.22E+07	4.71E-07	6.837E+13	875	3.13E+07	4.57E-07	6.84E+13
325	3.21E+07	4.70E-07	6.84E+13	880	3.12E+07	4.56E-07	6.85E+13
330	3.20E+07	4.67E-07	6.84E+13	885	3.14E+07	4.60E-07	6.84E+13
335	3.22E+07	4.70E-07	6.841E+13	890	3.11E+07	4.55E-07	6.84E+13
340	3.22E+07	4.70E-07	6.841E+13	895	3.11E+07	4.54E-07	6.84E+13
345	3.23E+07	4.72E-07	6.839E+13	900	3.13E+07	4.58E-07	6.84E+13
350	3.20E+07	4.68E-07	6.842E+13	905	3.14E+07	4.59E-07	6.84E+13
355	3.22E+07	4.71E-07	6.839E+13	910	3.10E+07	4.54E-07	6.84E+13
360	3.21E+07	4.69E-07	6.839E+13	915	3.11E+07	4.55E-07	6.84E+13
365	3.19E+07	4.67E-07	6.838E+13	920	3.11E+07	4.55E-07	6.84E+13
370	3.22E+07	4.71E-07	6.838E+13	925	3.11E+07	4.54E-07	6.84E+13
375	3.22E+07	4.71E-07	6.843E+13	930	3.10E+07	4.54E-07	6.84E+13
380	3.19E+07	4.67E-07	6.84E+13	935	3.12E+07	4.56E-07	6.85E+13
385	3.20E+07	4.68E-07	6.841E+13	940	3.10E+07	4.53E-07	6.84E+13
390	3.19E+07	4.67E-07	6.842E+13	945	3.12E+07	4.56E-07	6.84E+13
395	3.20E+07	4.68E-07	6.843E+13	950	3.11E+07	4.54E-07	6.84E+13
400	3.19E+07	4.66E-07	6.843E+13	955	3.10E+07	4.54E-07	6.84E+13
405	3.20E+07	4.68E-07	6.838E+13	960	3.10E+07	4.52E-07	6.84E+13
410	3.18E+07	4.65E-07	6.842E+13	965	3.10E+07	4.53E-07	6.84E+13
415	3.19E+07	4.67E-07	6.841E+13	970	3.10E+07	4.54E-07	6.84E+13
420	3.18E+07	4.64E-07	6.843E+13	975	3.10E+07	4.53E-07	6.84E+13
425	3.17E+07	4.64E-07	6.836E+13	980	3.10E+07	4.52E-07	6.84E+13

430	3.19E+07	4.66E-07	6.842E+13	985	3.09E+07	4.52E-07	6.84E+13
435	3.19E+07	4.66E-07	6.837E+13	990	3.11E+07	4.55E-07	6.85E+13
440	3.20E+07	4.68E-07	6.842E+13	995	3.10E+07	4.53E-07	6.84E+13
445	3.20E+07	4.68E-07	6.841E+13	1000	3.09E+07	4.52E-07	6.84E+13
450	3.22E+07	4.70E-07	6.84E+13	1005	3.11E+07	4.54E-07	6.84E+13
455	3.20E+07	4.68E-07	6.842E+13	1010	3.13E+07	4.57E-07	6.84E+13
460	3.21E+07	4.70E-07	6.841E+13	1015	3.11E+07	4.55E-07	6.84E+13
465	3.19E+07	4.67E-07	6.843E+13	1020	3.11E+07	4.55E-07	6.84E+13
470	3.19E+07	4.66E-07	6.844E+13	1025	3.09E+07	4.51E-07	6.84E+13
475	3.19E+07	4.66E-07	6.844E+13	1030	3.09E+07	4.52E-07	6.84E+13
480	3.20E+07	4.68E-07	6.839E+13	1035	3.09E+07	4.52E-07	6.84E+13
485	3.18E+07	4.65E-07	6.84E+13	1040	3.10E+07	4.53E-07	6.84E+13
490	3.17E+07	4.64E-07	6.834E+13	1045	3.10E+07	4.53E-07	6.84E+13
495	3.19E+07	4.66E-07	6.842E+13	1050	3.11E+07	4.54E-07	6.84E+13
500	3.18E+07	4.65E-07	6.84E+13	1055	3.11E+07	4.54E-07	6.84E+13
505	3.17E+07	4.64E-07	6.843E+13	1060	3.11E+07	4.54E-07	6.84E+13
510	3.17E+07	4.63E-07	6.841E+13	1065	3.11E+07	4.54E-07	6.84E+13
515	3.18E+07	4.65E-07	6.842E+13	1070	3.09E+07	4.52E-07	6.84E+13
520	3.15E+07	4.61E-07	6.842E+13	1075	3.08E+07	4.50E-07	6.84E+13
525	3.16E+07	4.62E-07	6.84E+13	1080	3.09E+07	4.52E-07	6.84E+13
530	3.15E+07	4.61E-07	6.843E+13				
535	3.17E+07	4.64E-07	6.844E+13				
540	3.18E+07	4.65E-07	6.843E+13				
545	3.17E+07	4.64E-07	6.84E+13				

Appendix 2: Table of the power analysis of the various cellophane sheets tested for the birefringence property. Included also is the power analysis of the commercial HWP for comparison.

Angle of rotation	Cello. A	Cello. B	Cello. C	Cello. D	Commercial HWP
0	9.62E+08	7.27E+08	8.06E+08	8.43E+08	7.94E+08
5	1.32E+10	1.15E+10	1.17E+10	9.32E+09	1.74E+10
10	5.35E+10	5.15E+10	5.36E+10	4.02E+10	7.12E+10
15	1.16E+11	1.15E+11	1.19E+11	8.87E+10	1.51E+11
20	1.92E+11	1.91E+11	2.00E+11	1.49E+11	2.49E+11
25	2.72E+11	2.71E+11	2.85E+11	2.13E+11	3.54E+11
30	3.49E+11	3.47E+11	3.67E+11	2.73E+11	4.49E+11
35	4.12E+11	4.09E+11	4.31E+11	3.21E+11	5.26E+11
40	4.52E+11	4.48E+11	4.73E+11	3.53E+11	5.75E+11
45	4.66E+11	4.62E+11	4.87E+11	3.64E+11	5.91E+11
50	4.52E+11	4.48E+11	4.72E+11	3.54E+11	5.71E+11
55	4.11E+11	4.07E+11	4.29E+11	3.23E+11	5.17E+11
60	3.49E+11	3.44E+11	3.64E+11	2.75E+11	4.37E+11
65	2.71E+11	2.68E+11	2.83E+11	2.15E+11	3.39E+11
70	1.90E+11	1.86E+11	1.98E+11	1.52E+11	2.35E+11
75	1.14E+11	1.11E+11	1.18E+11	9.15E+10	1.39E+11
80	5.11E+10	4.88E+10	5.32E+10	4.31E+10	6.01E+10
85	1.17E+10	1.00E+10	1.14E+10	1.08E+10	1.24E+10
90	8.55E+08	7.28E+08	8.28E+08	8.58E+08	7.36E+08
95	1.26E+10	1.35E+10	1.38E+10	6.61E+09	1.73E+10
100	5.39E+10	5.56E+10	5.81E+10	3.38E+10	7.11E+10
105	1.17E+11	1.21E+11	1.25E+11	7.88E+10	1.51E+11
110	1.95E+11	1.99E+11	2.07E+11	1.36E+11	2.49E+11
115	2.78E+11	2.82E+11	2.93E+11	1.97E+11	3.53E+11
120	3.55E+11	3.58E+11	3.75E+11	2.55E+11	4.48E+11
125	4.19E+11	4.21E+11	4.39E+11	3.02E+11	5.24E+11
130	4.59E+11	4.59E+11	4.82E+11	3.34E+11	5.72E+11
135	4.72E+11	4.72E+11	4.96E+11	3.46E+11	5.88E+11
140	4.58E+11	4.56E+11	4.81E+11	3.37E+11	5.67E+11

145	4.16E+11	4.14E+11	4.37E+11	3.08E+11	5.14E+11
150	3.53E+11	3.51E+11	3.72E+11	2.62E+11	4.34E+11
155	2.75E+11	2.74E+11	2.89E+11	2.04E+11	3.36E+11
160	1.92E+11	1.91E+11	2.03E+11	1.42E+11	2.33E+11
165	1.15E+11	1.14E+11	1.21E+11	8.36E+10	1.37E+11
170	5.07E+10	5.11E+10	5.52E+10	3.73E+10	5.88E+10
175	1.13E+10	1.14E+10	1.23E+10	7.73E+09	1.18E+10
180	9.22E+08	6.97E+08	7.61E+08	8.59E+08	7.98E+08
185	1.36E+10	1.19E+10	1.25E+10	9.86E+09	1.85E+10
190	5.58E+10	5.21E+10	5.52E+10	4.13E+10	7.35E+10
195	1.18E+11	1.16E+11	1.21E+11	9.02E+10	1.54E+11
200	1.95E+11	1.92E+11	2.01E+11	1.50E+11	2.53E+11
205	2.76E+11	2.72E+11	2.86E+11	2.13E+11	3.57E+11
210	3.51E+11	3.47E+11	3.67E+11	2.71E+11	4.52E+11
215	4.11E+11	4.08E+11	4.30E+11	3.18E+11	5.28E+11
220	4.49E+11	4.46E+11	4.72E+11	3.49E+11	5.76E+11
225	4.61E+11	4.58E+11	4.86E+11	3.58E+11	5.91E+11
230	4.45E+11	4.43E+11	4.70E+11	3.47E+11	5.69E+11
235	4.02E+11	4.02E+11	4.27E+11	3.15E+11	5.15E+11
240	3.39E+11	3.39E+11	3.61E+11	2.67E+11	4.34E+11
245	2.62E+11	2.64E+11	2.81E+11	2.08E+11	3.36E+11
250	1.82E+11	1.83E+11	1.95E+11	1.46E+11	2.32E+11
255	1.07E+11	1.08E+11	1.15E+11	8.82E+10	1.36E+11
260	4.65E+10	4.71E+10	5.13E+10	4.07E+10	5.94E+10
265	9.45E+09	9.43E+09	1.08E+10	9.97E+09	1.16E+10
270	8.86E+08	7.28E+08	8.08E+08	8.54E+08	7.58E+08
275	1.50E+10	1.39E+10	1.43E+10	6.68E+09	1.81E+10
280	5.84E+10	5.61E+10	5.83E+10	3.37E+10	7.21E+10
285	1.23E+11	1.21E+11	1.26E+11	7.76E+10	1.53E+11
290	2.01E+11	1.99E+11	2.08E+11	1.33E+11	2.51E+11
295	2.83E+11	2.81E+11	2.95E+11	1.93E+11	3.54E+11
300	3.59E+11	3.57E+11	3.75E+11	2.49E+11	4.50E+11
305	4.20E+11	4.19E+11	4.41E+11	2.96E+11	5.26E+11
310	4.59E+11	4.58E+11	4.84E+11	3.27E+11	5.75E+11
315	4.72E+11	4.72E+11	4.99E+11	3.39E+11	5.90E+11
320	4.56E+11	4.56E+11	4.84E+11	3.30E+11	5.70E+11
325	4.14E+11	4.14E+11	4.41E+11	3.02E+11	5.17E+11

330	3.51E+11	3.51E+11	3.76E+11	2.58E+11	4.37E+11
335	2.73E+11	2.74E+11	2.93E+11	2.02E+11	3.39E+11
340	1.91E+11	1.91E+11	2.06E+11	1.41E+11	2.36E+11
345	1.14E+11	1.15E+11	1.24E+11	8.40E+10	1.39E+11
350	5.15E+10	5.17E+10	5.74E+10	3.76E+10	6.13E+10
355	1.18E+10	1.17E+10	1.34E+10	8.11E+09	1.28E+10
360	9.74E+08	6.76E+08	7.46E+08	8.33E+08	7.58E+08

Appendix 3: A section of the MATLAB code used to evaluate the Stokes polarization parameters.

```
clear all
%% calculates the stokes parameters:
% Paper: 'Measuring the Stokes polarization parameters' Schaefer
% number of images / 180° N
N=16;

%% load reference
ref=load('reference.txt');
%% load all images
for p=1:N
    M(:,:,p)=double(imread(['Angle' int2str(p) '.bmp']))/ref(p);%
reference
end
```

```
%% determine angles
theta= 0:pi/N:pi; %pi/N is the interval

%% calculate the parameters A, B, C, D
A=0;
B=0;
C=0;
D=0;
for p=1:N
    A = A + M(:,:,p);
    B = B + M(:,:,p)*sin(2*theta(p));
    C = C + M(:,:,p)*cos(4*theta(p));
    D = D + M(:,:,p)*sin(4*theta(p));
end
```

```
A=A*2/N;
B=B*4/N;
C=C*4/N;
D=D*4/N;
```

```
%% calculate stokes images from A, B, C, D
S0=A-C;
S1=2*C;
S2=2*D;
S3=B;
```

```
%% calculate parameters from A, B, C, D
S0_abs=sum(sum(S0))/sum(sum(S0));% Normalizes to a unit
S1_abs=sum(sum(S1))/sum(sum(S0));
S2_abs=sum(sum(S2))/sum(sum(S0));
S3_abs=sum(sum(S3))/sum(sum(S0));
```

Appendix 4: A photograph of a section of the setup shown in figure 3.7 with some optical elements mounted on an optical table.

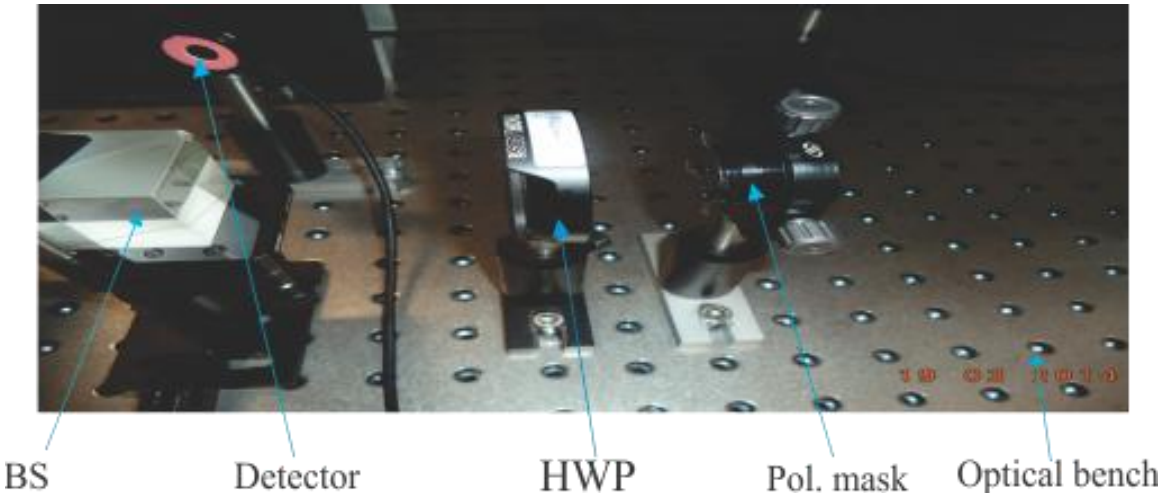

Appendix 5: A section of the data sheet for the commercial half wave plate used for comparison with cellophane.

THORLABS INC. PO BOX 366 NEWTON NJ

TITLE: 25.4mm, MOUNTED ZERO-ORDER COMPOUND WAVE PLATE, λ/2 WAVE @ 633nm

NOTES/SPECIFICATIONS:

1. UNMOUNTED DIAMETER: 1.00"±0.008 (25.4mm ±0.2)
2. BEAM DEVIATION: < 10 arcsec
3. RETARDANCE ACCURACY (TYP): < λ/300
4. TRANSMITTED WAVEFRONT ERROR: < λ/4
5. SURFACE QUALITY: 20-10 SCRATCH-DIG
6. CLEAR APERTURE: 0.89" (22.6mm)
7. COATING: VAR AT 633nm, R< 0.25%, 0° AOI